Cell Reports
Medicine

Report

SARS-CoV-2 antibodies from children exhibit broad neutralization and belong to adult public clonotypes

Graphical abstract

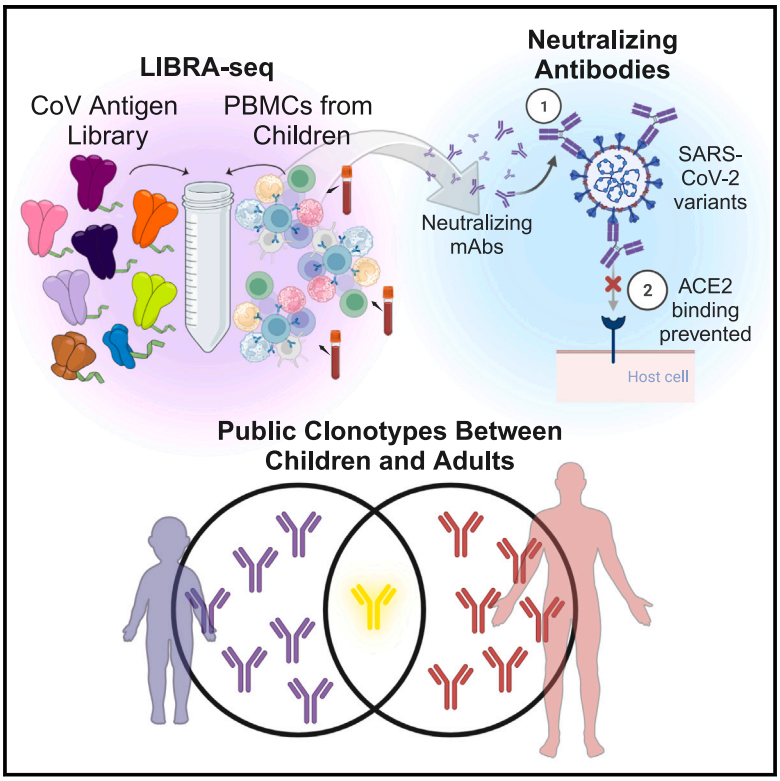

Highlights

- Applied LIBRA-seq to isolate cross-reactive coronavirus (CoV) B cells from children
- Identified a potent antibody against diverse SARS-CoV-2 variants, including XBB.1.5
- CoV antibodies from children and adults exhibited similar/public sequence signatures

Authors

Steven C. Wall, Naveenchandra Suryadevara, Changil Kim, ..., Daniel J. Sheward, Robert H. Carnahan, Ivelin S. Georgiev

Correspondence

ivelin.georgiev@vanderbilt.edu

In brief

Wall et al. demonstrate that SARS-CoV-2-reactive antibodies isolated from children can potently neutralize a broad range of virus variants, including highly neutralization-resistant XBB1.5, and can exhibit similar (public) genetic signatures compared to antibodies isolated from adults.

Wall et al., 2023, Cell Reports Medicine *4*, 101267
November 21, 2023
https://doi.org/10.1016/j.xcrm.2023.101267

CellPress

Cell Reports Medicine

CellPress
OPEN ACCESS

Report

SARS-CoV-2 antibodies from children exhibit broad neutralization and belong to adult public clonotypes

Steven C. Wall,[1,2] Naveenchandra Suryadevara,[1,10] Changil Kim,[3,10] Andrea R. Shiakolas,[1,2,10] Clinton M. Holt,[1,4] Emma B. Irbe,[1] Perry T. Wasdin,[1,4] Yukthi P. Suresh,[1] Elad Binshtein,[1] Elaine C. Chen,[1,2] Seth J. Zost,[1,2] Elizabeth Canfield,[2] James E. Crowe, Jr.,[1,2,5] Mary Ann Thompson-Arildsen,[2] Daniel J. Sheward,[3] Robert H. Carnahan,[1,5] and Ivelin S. Georgiev[1,2,6,7,8,9,11,*]

[1]Vanderbilt Vaccine Center, Vanderbilt University Medical Center, Nashville, TN 37232, USA
[2]Department of Pathology, Microbiology, and Immunology, Vanderbilt University Medical Center, Nashville, TN, USA
[3]Department of Microbiology, Tumor and Cell Biology, Karolinska Institutet, 171 65 Stockholm, Sweden
[4]Program in Chemical and Physical Biology, Vanderbilt University Medical Center, Nashville, TN, USA
[5]Department of Pediatrics, Vanderbilt University Medical Center, Nashville, TN, USA
[6]Vanderbilt Institute for Infection, Immunology, and Inflammation, Vanderbilt University Medical Center, Nashville, TN, USA
[7]Department of Computer Science, Vanderbilt University, Nashville, TN, USA
[8]Center for Structural Biology, Vanderbilt University, Nashville, TN, USA
[9]Program in Computational Microbiology and Immunology, Vanderbilt University Medical Center, Nashville, TN, USA
[10]These authors contributed equally
[11]Lead contact
*Correspondence: ivelin.georgiev@vanderbilt.edu
https://doi.org/10.1016/j.xcrm.2023.101267

SUMMARY

From the beginning of the COVID-19 pandemic, children have exhibited different susceptibility to severe acute respiratory syndrome coronavirus 2 (SARS-CoV-2) infection, reinfection, and disease compared with adults. Motivated by the established significance of SARS-CoV-2-neutralizing antibodies in adults, here we characterize SARS-CoV-2-specific antibody repertoires in a young cohort of individuals aged from 5 months to 18 years old. Our results show that neutralizing antibodies in children possess similar genetic features compared to antibodies identified in adults, with multiple antibodies from children belonging to previously established public antibody clonotypes in adults. Notably, antibodies from children show potent neutralization of circulating SARS-CoV-2 variants that have cumulatively resulted in resistance to virtually all approved monoclonal antibody therapeutics. Our results show that children can rely on similar SARS-CoV-2 antibody neutralization mechanisms compared to adults and are an underutilized source for the discovery of effective antibody therapeutics to counteract the ever-evolving pandemic.

INTRODUCTION

The human immune response to a pathogen depends on a wide variety of factors, including the history of prior exposure to the same or related pathogens, as well as the current state of an individual's immune system. Compared with adults, children's infection and vaccination histories are more limited, and their immune systems are not fully mature. As a result, substantial differences in disease phenotype can be observed for a variety of infectious diseases between children and adults.[1–3] In particular, children tend to be more susceptible to severe disease phenotypes for several common infectious diseases, including influenza, respiratory syncytial virus, human metapneumovirus, and others.[1–3] However, this trend appeared to be reversed in the case of severe acute respiratory syndrome coronavirus 2 (SARS-CoV-2), with children experiencing significantly less severe disease phenotypes compared with adults.[4,5] Adolescents also have less incidence of severe COVID-19, and those with severe disease exhibit lower rates of hospitalization, require shorter hospital stays, and have lower mortality than adults.[6] While there have been some efforts aiming to understand these differences in how children and adults respond to SARS-CoV-2 infection, little is still known about the specific factors that are responsible for this phenomenon.

While a number of immune system components have been implicated in the response to SARS-CoV-2 infection and vaccination,[7–9] antibodies that are capable of effectively neutralizing the virus are among the most critical factors.[10] In fact, the elicitation of neutralizing antibodies to the spike glycoprotein of SARS-CoV-2 is the primary target for the majority of current vaccines on the market.[11,12] The initial SARS-CoV-2 vaccine candidates were developed based on the knowledge that neutralizing antibodies previously had been shown to protect against infection with a variety of other pathogens,[13] long before ultimately

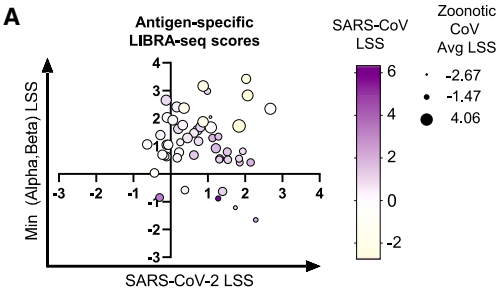

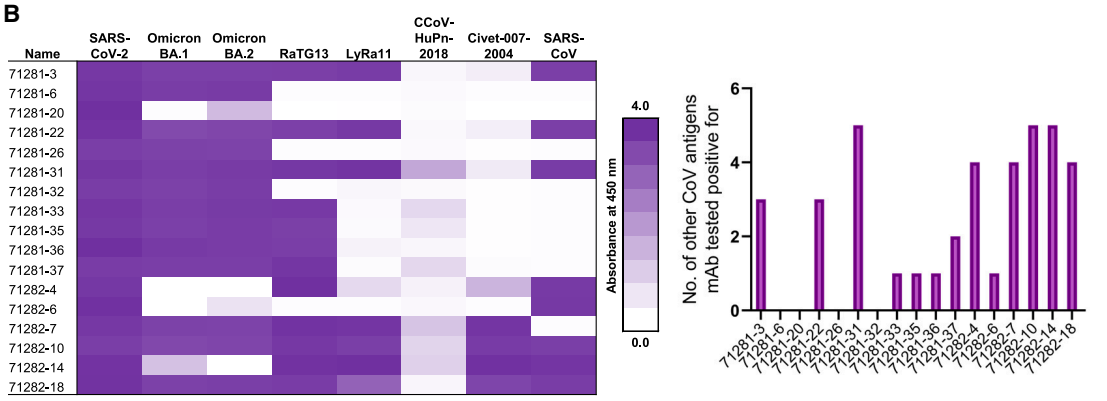

C

Name	VH gene	JH gene	VH identity	JH identity	Native isotype	CDRH3 sequence	CDRH3 length	VL gene	JL gene	VL identity	JL identity	CDRL3 sequence	CDRL3 length
71281-3	*IGHV3-7*	*IGHJ4*	0.97	0.92	IGHG1	VSCSSSSWEFDY	12	*IGLV3-1*	*IGLJ2*	0.95	0.94	QAWASSTAI	9
71281-6	*IGHV3-30*	*IGHJ4*	0.95	0.88	IGHA1	ARSPGTAWGGYMDV	14	*IGKV1-33*	*IGKJ3*	0.97	0.97	QQYENLIFT	9
71281-20	*IGHV3-74*	*IGHJ5*	0.93	0.94	IGHG1	ARQFLRGVVINWFGP	15	*IGKV4-1*	*IGKJ1*	0.98	0.91	QQYYTTPE	9
71281-22	*IGHV4-31*	*IGHJ6*	0.97	0.90	IGHG1	ARALGDLPYYYYGLDV	16	*IGLV1-44*	*IGLJ1*	0.98	1.00	ATWDDSLSGLYV	12
71281-26	*IGHV3-23*	*IGHJ2*	0.94	0.94	IGHA1	VSPGDNVPDWYFDL	14	*IGLV2-14*	*IGLJ3*	0.94	1.00	YSLTTTTTWV	10
71281-31	*IGHV3-30*	*IGHJ4*	0.97	0.90	IGHA1	AKDPTARLGYCRGGSCYLADY	21	*IGLV3-21*	*IGLJ2*	0.97	0.97	QVWESSSDHVI	11
71281-32	*IGHV2-5*	*IGHJ4*	0.98	0.81	IGHA1	VHHTITMIVGY	11	*IGLV2-14*	*IGLJ2*	0.98	0.97	SSYTTSSVV	9
71281-33	*IGHV3-66*	*IGHJ4*	0.94	0.94	IGHG1	ARGFGDHYFNS	11	*IGKV1-5*	*IGKJ2*	0.96	1.00	QQYNTYT	7
71281-35	*IGHV3-53*	*IGHJ5*	0.98	0.84	IGHG1	ARETPGYGDEA	11	*IGKV1-33*	*IGKJ2*	0.99	1.00	QQYDNLPRT	9
71281-36	*IGHV1-58*	*IGHJ3*	0.95	0.90	IGHA1	AAPNCTGGSCFDGFNL	16	*IGKV3-20*	*IGKJ2*	0.94	0.97	QQYSRSPYS	9
71281-37	*IGHV3-53*	*IGHJ1*	0.94	0.81	IGHG1	ARGPYCRGAGCRP	13	*IGKV1-33*	*IGKJ5*	0.98	0.92	QQYDNLPMT	9
71282-4	*IGHV1-69*	*IGHJ4*	0.97	0.90	IGHA2	ANDYTSSGWYTPLDY	15	*IGKV1-17*	*IGKJ1*	0.97	0.95	LQHNNYPWT	9
71282-6	*IGHV3-48*	*IGHJ3*	0.95	0.96	IGHG1	ARDGDYYDSSGHSREAFDI	19	*IGLV1-36*	*IGLJ3*	0.99	0.97	ATWDDSLNAWV	11
71282-7	*IGHV3-30-3*	*IGHJ5*	0.95	0.96	IGHG1	ARAGGGTYYSWFDP	14	*IGKV3-20*	*IGKJ3*	0.99	0.95	QHYGSSFT	8
71282-10	*IGHV3-30*	*IGHJ3*	0.95	0.92	IGHA1	ARAYGGSYSGAFDI	14	*IGKV3-20*	*IGKJ2*	0.98	1.00	QQYGSSPMYT	10
71282-14	*IGHV3-30*	*IGHJ4*	0.99	0.81	IGHG1	AAVVDIVVVPSIILLPPDY	19	*IGLV1-47*	*IGLJ1*	0.98	1.00	AAWDDSLSGYV	10
71282-18	*IGHV4-59*	*IGHJ3*	0.99	0.98	IGHG3	ARTYYYDRSGPTHAFDI	17	*IGKV2D-29*	*IGKJ2*	0.99	1.00	MQNIQLLYT	9

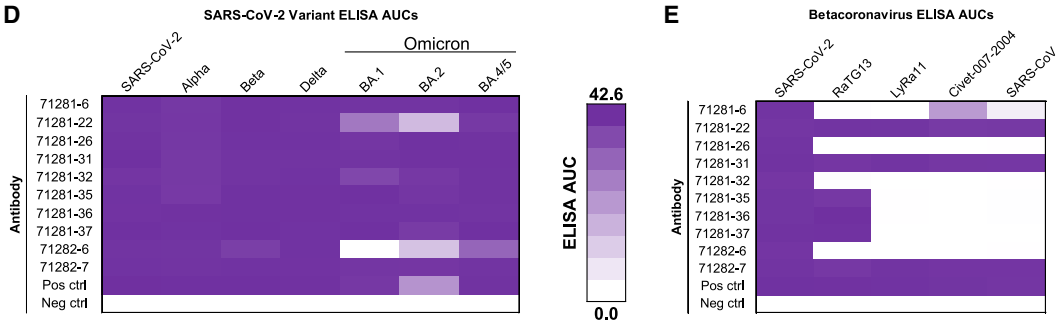

Figure 1. Using LIBRA-seq with a diverse CoV antigen panel to discover antibodies from children's samples

(A) 59 IgG and IgA cells identified by LIBRA-seq are shown as circles, with their respective LIBRA-seq scores (LSSs) for SARS-CoV-2 (x axis), minimum score for the Alpha and Beta SARS-CoV-2 variants (y axis), and SARS-CoV (color heatmap) and average score for the potentially zoonotic CoV spikes used in the LIBRA-seq library (size of circle).

(B) Recombinant antibodies were produced by microexpression and screened by ELISA against a panel of recombinant CoV spike antigens. For the antibodies that were positive for SARS-CoV-2 spike binding, shown are (left) a binding heatmap for each antibody (rows) against a panel of SARS-CoV-2 variants and other coronaviruses (columns) and (right) the number of non-SARS-CoV-2 antigens (y axis) that each antibody (x axis) was able to recognize.

(legend continued on next page)

showing that such antibodies are a correlate of protection against SARS-CoV-2 as well.[10,14] Antibody responses to SARS-CoV-2 infection and vaccination have been extensively studied in adults, resulting in a plethora of information about the genetic, molecular, and functional characteristics of SARS-CoV-2-specific antibodies.[8,12,15,16] While antibodies in adults have been found to target a variety of different epitopes on the spike glycoprotein, several epitope clusters have been identified that are commonly targeted at the population level.[17] Importantly, the ability of different individuals to target similar epitopes is in part attributed to the existence of ''public'' antibodies with highly similar genetic features that are found in many individuals.[18,19] In practice, public antibodies in the context of SARS-CoV-2 have been defined based on the use of identical combinations of variable heavy (VH) and variable light (VL) genes,[8,20] although more stringent requirements related to high sequence identity in the third complementarity-determining regions of the heavy and light chains (CDRH3 and CDRL3, respectively) can also be incorporated.[18,19] Overall, the identification of a variety of public antibodies indicates that the immune system in adults can converge on a few common modes of SARS-CoV-2 spike recognition that can effectively counteract the virus.

Within the first few months of the pandemic, monoclonal antibodies (mAbs) isolated from adults were translated into the clinic as both preventive and therapeutic measures.[21–28] The critical significance of translating multiple mAbs with different genetic, epitope, and functional characteristics into the clinic became especially evident once the effects of SARS-CoV-2 variant evolution came to the forefront. While the approved mAbs were initially effective against the wild-type virus, mutations within the spike protein soon enabled viral escape from some, and now virtually all, mAbs on the market.[29–36] Further efforts toward the development of next-generation mAbs with an expanded breadth of SARS-CoV-2 variant reactivity is currently ongoing.[37–39]

Unlike the expansive studies of antibody responses to SARS-CoV-2 in adults, there is little to no information about the types and specificities of neutralizing antibodies in children, with studies generally limited to the assessment of polyclonal responses.[40–42] To address this, we employed LIBRA-seq (linking B cell receptor to antigen specificity through sequencing), a powerful tool that combines a DNA oligo barcoded antigen library, fluorescence-activated cell sorting (FACS), next-generation sequencing (NGS), and a computational pipeline to enable high-throughput mapping of antibody sequence to antigen specificity while maintaining single-cell resolution with high precision.[43] Peripheral blood mononuclear cells (PBMCs) from children are generally challenging to acquire, and LIBRA-seq facilitated the utilization of limited samples to efficiently discover cross-reactive B cells predicted to bind the spike protein of SARS-CoV-2, its variants, and other betacoronaviruses. Due to the different disease phenotypes observed in children compared with adults and the established significance of the antibody response to SARS-CoV-2 in adults, we set out to explore the characteristics of SARS-CoV-2-specific antibodies in children. In this work, we aimed to delineate similarities and differences between SARS-CoV-2 antibodies in children and previously characterized antibody responses in adults, focusing on both genetic features and functional characteristics like epitope specificity and neutralization phenotypes. The results presented here highlight the properties of SARS-CoV-2-specific antibody responses in children and emphasize the potential of samples from children as an underutilized source for clinical mAb candidates and can help inform the design of next-generation pediatric vaccines.

RESULTS

Cohort of samples from children

We obtained PBMCs from peripheral blood samples remaining after diagnostic tests were performed in the Clinical Hematology Laboratory at Vanderbilt University Medical Center (VUMC). Samples were collected for children up to 18 years of age between July and August 2021. Samples were divided into two groups: 71281, no known exposure to SARS-CoV-2 infection or vaccination, and 71282, known exposure to SARS-CoV-2 infection or vaccination, determined through self-reporting. Group 1 included a total of 44 samples, with ages ranging from 5 months to 17 years, and a median age of 9.5, while group 2 included a total of 12 samples, with ages ranging from 13 to 18 years, and a median age of 15.5 (Figure S1). Due to low sample volumes (ranging from 200 μL to 3 mL, average ~1 mL), all samples within a group were pooled together for subsequent characterization.

Discovery of SARS-CoV-2 antibodies from children's samples

For each of the two sample groups, we performed a LIBRA-seq discovery experiment to determine the cross-reactivity patterns of SARS-CoV-2+ B cells from children. The antigen screening library incorporated a panel of stabilized recombinant spike antigens from SARS-CoV-2 variants (WA1, Alpha, and Beta) and from other sarbecoviruses with potential for zoonosis (SARS-CoV, RaTG13, LYRa11, and Civet-007-2004). Applying this antigen library to the two groups of samples described above resulted in the identification of a number of B cells with predicted cross-reactivity between multiple SARS-CoV-2 variants, multiple sarbecoviruses, or both (Figure 1A). Based on these LIBRA-seq results, a set of B cells were prioritized for further characterization as recombinant immunoglobulin G1 (IgG1) mAbs. Microscale expression of paired heavy-light chains (see STAR Methods), followed by antigenicity characterization by ELISA, revealed 17 antibodies with breadth within SARS-CoV-2 and/or other non-SARS-CoV-2 coronavirus recognition from each of the two groups of samples (Figure 1B). These antibodies derived from multiple different isotypes (IgG1, IgG3, and

(C) For each antibody (rows), shown are the CDR amino acid sequences and lengths, V-gene and J-gene and percentage of nucleotide identities, and isotype (columns).

(D and E) ELISA area under the curve (AUC) values from purified monoclonal antibody binding to (D) SARS-CoV-2 variant spike proteins and (E) other betacoronavirus spike proteins are shown as heatmaps from minimum (white) to maximum (purple) binding. ELISA controls are described in Figure S2.

IgA1) and utilized diverse heavy- and light-chain variable genes with varying CDRH3 and CDRL3 lengths (CDRH3: 11–21 amino acids; CDRL3: 7–12 amino acids) and somatic hypermutation levels (heavy chain: 1%–7%; light chain: 1%–6%) (Figure 1C). Antibody leads were then expressed in large scale, purified, and tested for recognition of an expanded set of antigens. The antibodies showed diverse antigen specificities, with recognition of different subsets of SARS-CoV-2 variants, including the omicron lineage variants BA.1, BA.2, and BA.4/5, (Figures 1D and S2) or other sarbecoviruses (Figures 1E and S2). Together, these results revealed the existence of SARS-CoV-2 antibodies in samples from children with a wide range of breadth within SARS-CoV-2 and related sarbecoviruses.

Antibodies from children neutralize recently emergent SARS-CoV-2 variants

We next sought to explore whether the SARS-CoV-2 antibodies identified from children's samples exhibit neutralization breadth and potency against diverse SARS-CoV-2 variants (Figure 2). Indeed, 8 of the 14 antibodies from children that showed binding to at least one SARS-CoV-2 variant or SARS-CoV, when tested in a vesicular stomatitis virus (VSV)-based neutralization assay,[44,45] potently neutralized the SARS-CoV-2 variant harboring the D614G mutation,[46] with a half maximal inhibitory concentration (IC_{50}) of <10 ng/mL observed for 3 antibodies (Figures 2A and S3A). Similar neutralization patterns were also observed against the D614G variant in a pseudotyped-virus-based neutralization assay (Figure 2B). The pseudotyped virus assay was also used for evaluating the breadth of the antibodies against recently emergent Omicron variants that have been associated with resistance to virtually all available mAb therapies.[33,34,36,47] Notably, 6 of the 7 antibodies from children exhibited neutralization breadth against 4 or more of the tested variants with IC_{50s} <1 μg/mL, and all of the tested antibodies neutralized BA.4/5 (Figure 2B). In particular, antibody 71281-33 retained neutralization potency against all 9 SARS-CoV-2 pseudovirus variants tested: D614G, BA.2, BA.2.75+R346T, BA.4, BA.4.6, BA.2.75.2, XBB, BQ.1.1, and XBB.1.5, the last 5 of which have been implicated in resistance to mAb neutralization, including to bebtelovimab, Evusheld (a cocktail of tixagevimab and cilgavimab), and sotrovimab.[33,34,36,47] Together, these data show that antibodies identified from children's samples can display high levels of neutralization breadth and potency against SARS-CoV-2 variants even without prior vaccination or exposure to that variant. More generally, these results indicate that children's samples can play an important role in the discovery of effective SARS-CoV-2 antibody therapeutics.

Antibodies from children target multiple diverse epitopes on the SARS-CoV-2 spike

To evaluate the breadth of epitopes targeted by antibodies from children, we first tested binding against different spike subdomains (Figures 3A and S2B). Both receptor-binding domain (RBD) and S2 subdomain antibodies were identified. Further, antibody competition for spike-receptor ACE2 binding was tested in an ELISA, revealing high levels (>85%) of ACE2-blocking activity by 7/10 RBD-specific antibodies and medium levels (25%–38%) of blocking activity by 2 of the remaining RBD-specific antibodies (Figure 3B). Notably, antibody 71281-31 showed strong ACE2-blocking ability against both SARS-CoV-2 and SARS-CoV, in line with the SARS-CoV/SARS-CoV-2 cross-reactivity (Figure 1E) and RBD recognition (Figure 3A) observed for this antibody. Antibody 71281-31 was also able to neutralize both SARS-CoV-2 (Figure 2A) and SARS-CoV (Figure S3B), albeit at low potency, indicating a potential trade-off between high breadth of virus recognition and neutralization potency. As a next step, we selected the exceptionally broadly SARS-CoV-2-neutralizing antibody 71281-33 and the SARS-CoV/SARS-CoV-2 cross-reactive antibody 71281-31 to further delineate their epitope regions in antibody competition assays, both against other antibodies from children, as well as against published adult SARS-CoV-2 antibodies (Figure 3C). Antibody 71281-31 did not compete with any other antibodies, including the published S309 RBD SARS-CoV/SARS-CoV-2-reactive antibody,[23] suggesting that it targets a unique cross-reactive epitope. In contrast, antibody 71281-33 competed with a subset of the other antibodies from children, and to some extent with the published class 1 RBD antibody CB6 (etesevimab),[25] but no other antibodies in the set that was tested. Next, we performed negative-stain electron microscopy (nsEM) experiments in order to further delineate the epitope of neutralizing antibody 71281-33. Reconstructive 3D mapping of the SARS-CoV-2 spike in complex with Fab 71281-33 indicated that the epitope of that antibody is near the receptor-binding motif (RBM) of the RBD. Notably, the nsEM reconstruction showed Fab 71281-33 binding to the RBD in both the up and down states (Figures S3C–S3E). This epitope, along with the IGHV3-66 gene usage, short CDRH3, and mild competition with CB6, indicates that mAb 71281-33 is likely a class 1 RBD antibody.[17] Together, these results suggest that the SARS-CoV-2 antibodies that we identified from children samples target a variety of different epitopes both on the spike in general and within the RBD subdomain.

Antibodies from children have sequence features that are associated with known public clonotypes in adults

Characterization of the antibody responses to SARS-CoV-2 infection and vaccination in adults has led to the discovery of common genetic characteristics for SARS-CoV-2-reactive antibodies that are observed in multiple individuals.[17,19,20,48,49] Such antibodies define public clonotypes and highlight a convergent mechanism of viral antigen recognition that can be observed at the population level.[17–20,42] We therefore set out to explore how similar the antibodies discovered here are compared to known SARS-CoV-2-reactive antibodies in adults. To that end, utilizing the genetic features identified in Figure 1C, we compared each of the SARS-CoV-2-reactive antibodies identified here to a database of published SARS-CoV-2 antibody sequences.[50] Notably, 16 of 17 antibodies that showed binding to SARS-CoV-2 spike utilized a combination of VH and VL chain genes that was identical to previously published adult SARS-CoV-2 antibodies (Figures 4A and S4). Of these, 11 antibodies also had CDRH3 identity of >50% to at least one published adult SARS-CoV-2 antibody, and 4 antibodies had CDRH3 identity of >70% (Figures 4A and S4). For all of the spike-binding antibodies from children, previously published SARS-CoV-2 antibodies were identified that utilized an identical VH chain gene, independent of the VL gene, with 15 of the antibodies having CDRH3 identity of >50% to at least one published

CellPress
OPEN ACCESS

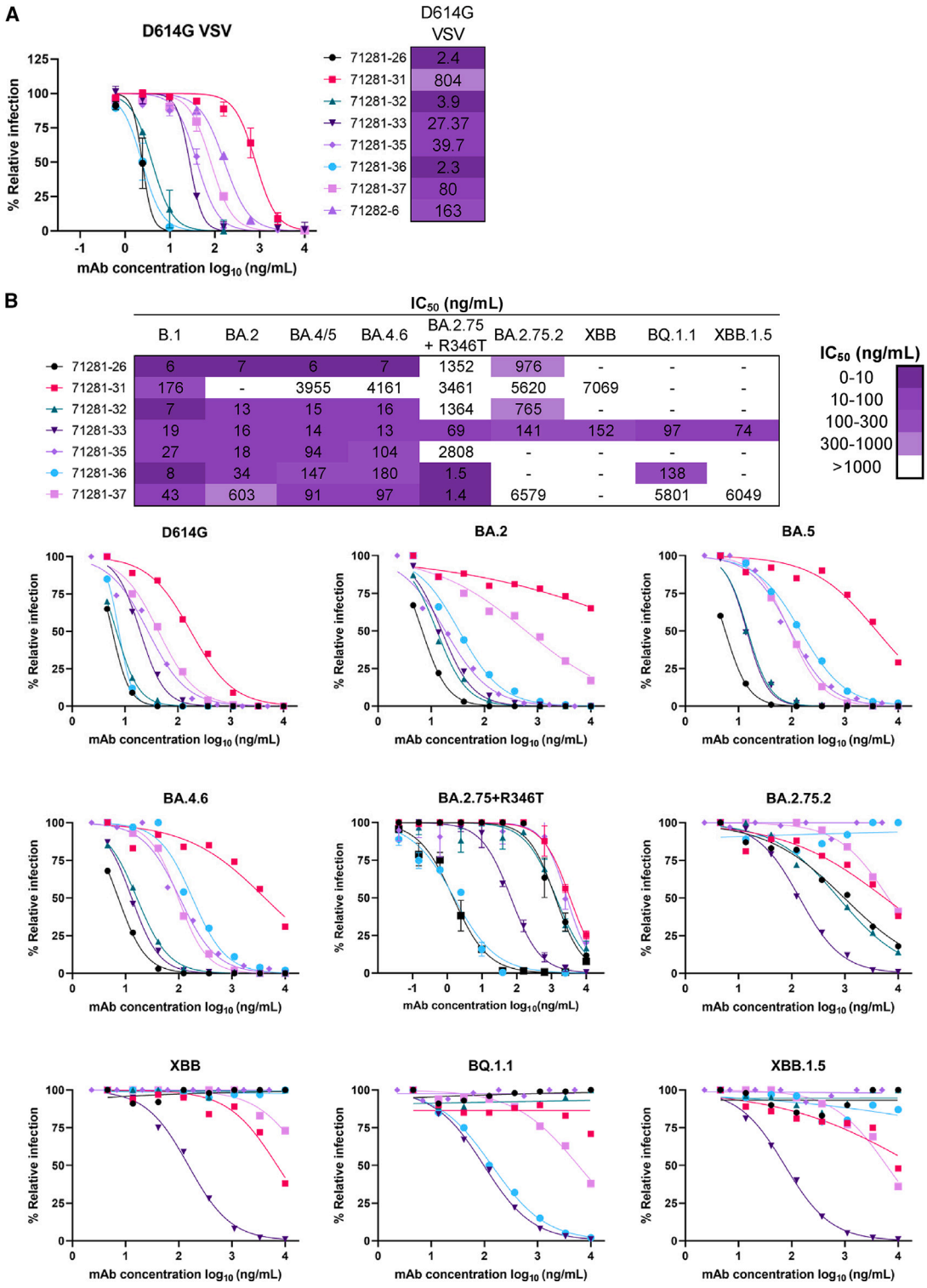

Figure 2. Antibodies from children show diverse neutralization profiles of SARS-CoV-2 variants

(A) SARS-CoV-2 VSV-G neutralization was performed for a panel of antibodies against SARS-CoV-2 VSV-G with the D614G mutation.

(B) Additional lentiviral pseudovirus neutralization assays were performed against SARS-CoV-2 D614G and Omicron variants (BA.2, BA.4/5, BA.4.6, BA.2.75.2, BA.2.75+R346T, XBB, XBB.1.5, and BQ1.1). The IC_{50} values calculated in GraphPad Prism software by four-parameter best-fit analysis are shown on the bottom right as a color heatmap from least (white) to most (purple) potent. Data represent the percentage of neutralization or relative infection as mean ± SD; data are representative of at least two independent experiments performed in technical duplicate.

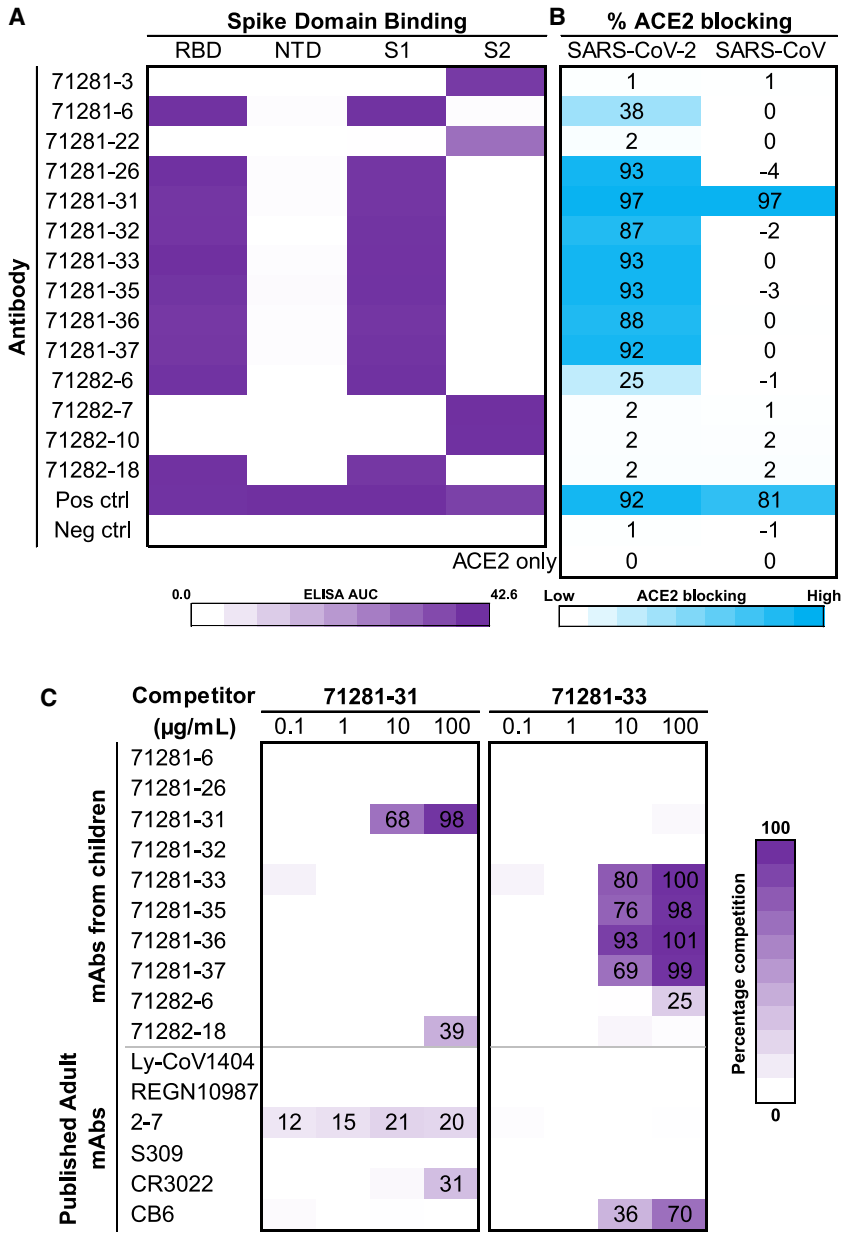

Figure 3. Epitope and ACE2-blocking analysis of antibodies from children

(A) ELISA AUC values for recombinant SARS-CoV-2 spike antigen domains are shown as heatmaps from minimum (white) to maximum (purple) binding. Controls are described in Figure S2B.

(B) Percentage of ACE2 blocking by ELISA is shown for SARS-CoV-2 and SARS-CoV spike proteins and is depicted as a heatmap from 0% (white) to 100% (blue).

(C) Antibody-antibody competition ELISAs were performed for antibodies 71281-31 and 71281-33 against other child antibodies identified here, as well as previously published adult antibodies. Percentage of competition is shown as a heatmap from 0% (white) to 100% (purple). Non-biotinylated competitor antibodies were coated first, and then biotinylated 71281-31 and 71281-33 were added to detect competition, as described in more detail in the STAR Methods.

adult SARS-CoV-2 antibody, and 5 antibodies had CDRH3 identity of >70% (Figures 4A and S4). Specifically focusing on the subset of 8 antibodies from children that were found to be neutralizing, all 8 utilized a combination of VH and VL genes that was identical to previously published adult SARS-CoV-2 antibodies, and 5 of the 8 also had CDRH3 identity of >50% to at least one published adult SARS-CoV-2 antibody (Figure 4A). Some of these combinations included well-documented public SARS-CoV-2 clonotypes that have been defined as public clonotypes specifically based on the variable gene usage, including IGHV1-58/IGKV3-20[19,51–53] (used by antibody 71281-36) and IGHV2-5/IGLV2-14[22,54,55] (utilized by 71281-32), as well as the IGHV3-53/3-66 public class of SARS-CoV-2 antibodies[19,53,56] (utilized by 71281-33, 71281-35, and 71281-37).

In addition to the large-scale database comparison, we also evaluated the similarity of the antibodies identified here to a set of marketed, in-development, or well-characterized SARS-CoV-2 antibodies. Of note, several of the antibodies from children belonged to the same clonotypes as these published mAbs. In particular, 71281-32 shared identical VH and VL chain gene usage with LY-CoV1404 (bebtelovimab) and 2-7, and 71281-36 shared identical VH and VL chain genes with tixagevimab, S2E12, and A23-58.1, with CDRH3 identities of 56%, 62%, and 75%, respectively (Figure 4B). Together, these results suggest that the development of SARS-CoV-2 antigen specificity may use similar antibody sequence solutions in children to those used in adults.

DISCUSSION

The state-of-the-art technologies that have revolutionized the field of antibody research in recent years have had limited applications in the context of children, likely due to the difficulty of obtaining and studying samples from children. Given the established importance of antibodies as a major component of immune responses to infection and vaccination, efforts aiming to fill this gap in knowledge can have significant implications for basic immunology, through shedding light on the fundamental rules that govern antigen recognition by antibodies in children. Such efforts can also be of clinical and translational significance by providing insights for the development of mAb therapies and vaccine modalities that are specifically tailored toward children.

Due to the significant differences in disease phenotype between children and adults, studying antigen-specific antibody repertoires in children in the context of SARS-CoV-2 is well

CellPress
OPEN ACCESS

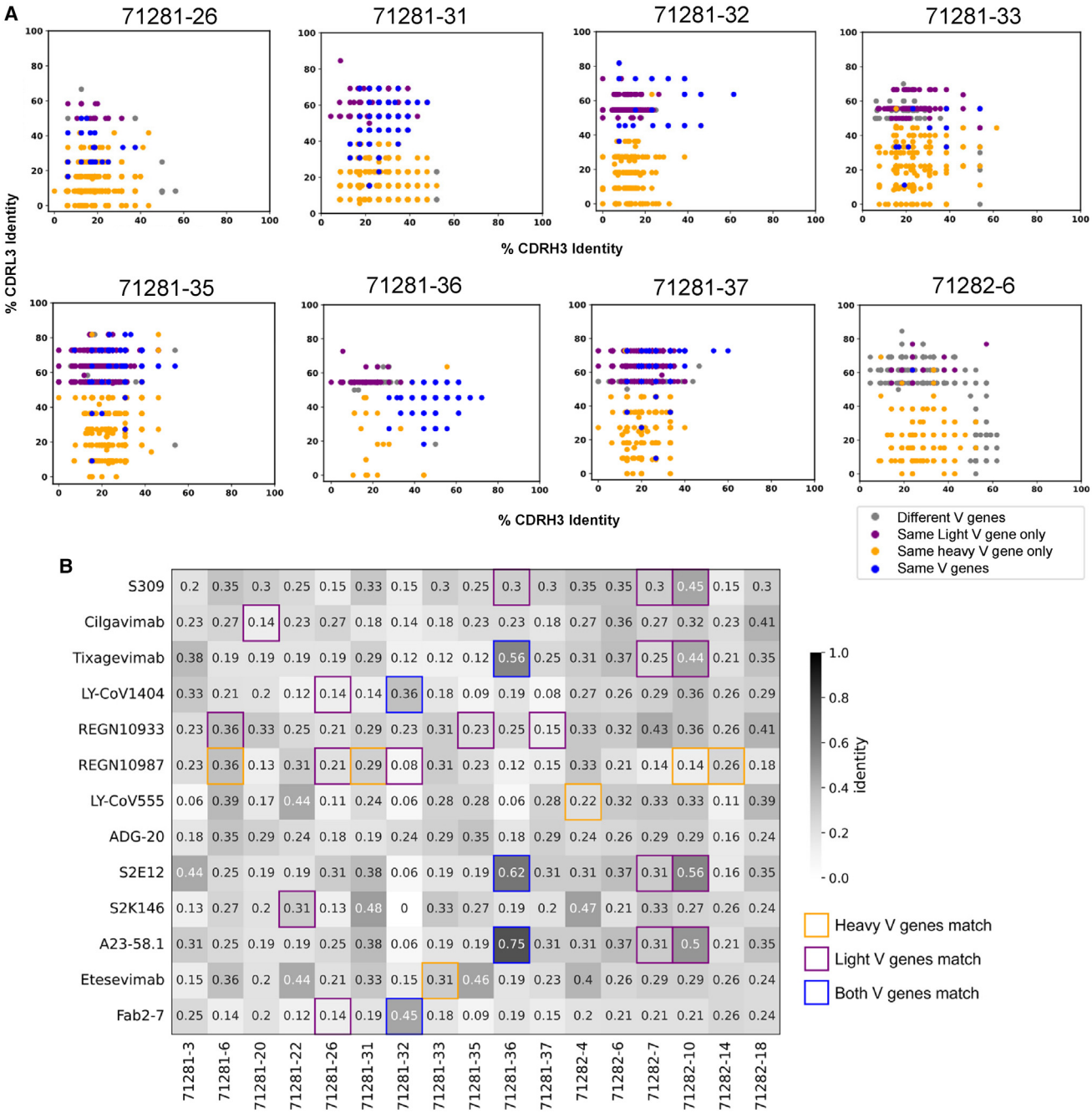

Figure 4. Public clonotype analysis of SARS-CoV-2 antibodies from children

(A) For each antibody from children (separate plot), shown are previously published adult antibodies (dots), with the respective CDRH3 (x axis) and CDRL3 (y axis) identity, colored according to V-gene usage: blue if both the VH and VL genes of the given child and adult antibodies match, orange if only the VH genes match, purple if only the VL genes match, and gray if neither match but at least one of the CDRH3 and CDRL3 have >50% sequence identity for the child vs. adult antibody.

(B) For each antibody from children (column), shown is the CDRH3 identity (values; heatmap) against a set of adult antibodies in clinical use or advanced preclinical development (rows). Cell border color corresponds to the V-gene usage described in (A).

motivated. To that end, using the LIBRA-seq technology for high-throughput antibody discovery, we identified and characterized a number of SARS-CoV-2-spike-specific antibodies from a cohort of children. Importantly, these antibodies targeted a variety of different spike epitopes and were associated with diverse genetic features, suggesting a broad portfolio of potential solutions for antigen targeting in children. Moreover, several of the antibodies from children belonged to known classes

of public antibodies from adults, suggesting that there is a convergence of antigen-specific antibody responses for a wide range of ages. We note, however, that while child and adult antibodies can belong to overlapping public clonotypes based on common variable gene usage, there can be sufficient differences in the antibody sequence (e.g., in the CDRH3 region; Figure 4A) that could lead to major differences in the neutralization sensitivity phenotypes for these antibodies (Figure 2B) compared with adult antibodies from the same public clonotypes. This indicates that optimization of the antibody neutralization phenotype can be achieved through fine-tuning of antigen recognition even within individual public clonotypes.[20,51,57,58]

Notably, a set of antibodies from children showed potent neutralization of different currently circulating SARS-CoV-2 variants, including variants that have successfully escaped from the currently available mAb products. This result points to samples from children as a potential source for the development of mAb candidates with improved breadth of SARS-CoV-2 reactivity and further highlights the importance of deciphering the antigen-specific antibody repertoires in children for other infectious diseases with high biomedical significance.

Limitations of the study

This study investigates the genetic features, antigen cross-reactivity, and coronavirus neutralization breadth of antibodies discovered in a cohort of children aged 5 months to 18 years. Due to the limited number of samples that we were able to obtain in the lower end of the age range (0–5 years), samples were pooled, and group 71282 consisted of samples from only adolescent ages 12–17. Future studies that include stratified children's age groups with retained donor source information for the identified B cells can better reflect the different characteristics of B cell repertoires in children. Additionally, while samples from group 71281 had no history of infection or vaccination, we were unable to experimentally confirm this, so we cannot rule out the possibility that donors in that cohort had been exposed at some point. Finally, public clonotype analysis was defined purely through sequence features. A comprehensive mapping of epitopes would need to be performed to confirm that adult and child antibodies that meet the sequence criteria to be defined within the same clonotype bind the spike protein in near-identical ways.

STAR★METHODS

Detailed methods are provided in the online version of this paper and include the following:

SUPPLEMENTAL INFORMATION

Supplemental information can be found online at https://doi.org/10.1016/j.xcrm.2023.101267.

ACKNOWLEDGMENTS

We thank A. Jones, L. Raju, and J. Roberson of VANTAGE for their expertise regarding NGS and library preparation; D. Flaherty and B. Matlock of the Vanderbilt Flow Cytometry Shared Resource for help with flow panel optimization; and members of the Georgiev laboratory for comments on the manuscript. The Vanderbilt VANTAGE Core provided technical assistance for this work. VANTAGE is supported, in part, by CTSA grant 5UL1 RR024975-03, the Vanderbilt-Ingram Cancer Center (P30 CA68485), the Vanderbilt Vision Center (P30 EY08126), and NIH/NCRR (G20 RR030956). This work was conducted, in part, using the resources of the Advanced Computing Center for Research and Education (ACCRE) at Vanderbilt University. Flow cytometry experiments were performed in the Vanderbilt University Medical Center (VUMC) Flow Cytometry Shared Resource. The VUMC Flow Cytometry Shared Resource is supported by the Vanderbilt-Ingram Cancer Center (P30 CA68485) and the Vanderbilt Digestive Disease Research Center (DK058404). EM data collections were conducted at the Center for Structural Biology Cryo-EM Facility at Vanderbilt University. The following reagent was obtained through BEI Resources, NIAID, NIH: human embryonic kidney cells (HEK-293T) expressing human angiotensin-converting enzyme 2, HEK-293T-hACE2 cell line, NR-52511. We thank the G2P-UK National Virology consortium funded by MRC/UKRI (MR/W005611/1) and the Barclay group at Imperial College for providing spike expression plasmids. For work described in this manuscript, I.S.G., S.C.W., A.R.S., C.M.H., P.T.W., and Y.P.S. were supported, in part, by NIH National Institute of Allergy and Infectious Diseases (NIAID) award R01 AI131722-S1, the Hays Foundation COVID-19 Research Fund, Fast Grants, and the G. Harold and Leila Y. Mathers Charitable Foundation. J.E.C., N.S., E.C.C., and R.H.C. were supported, in part, by Defense Advanced Research Projects Agency (DARPA) grant HR0011-18-2-0001, US NIH contract 75N93019C00074, NIH grant R01 AI157155, the Dolly Parton COVID-19 Research Fund at Vanderbilt, and a grant from Fast Grants, Mercatus Center, George Mason University. J.E.C. is a recipient of the 2019 Future Insight Prize from Merck KGaA, which supported this work with a grant. The graphical abstract was created using BioRender.com.

AUTHOR CONTRIBUTIONS

S.C.W., A.R.S., and I.S.G. developed the methodology. S.C.W., N.S., C.K., A.R.S., C.M.H., E.B.I., P.T.W., Y.P.S., S.J.Z., E.C.C., E.B., and D.J.S. performed the investigations. E.C. and M.A.T.-A. provided blood samples from children. S.C.W. performed validations. S.C.W. and I.S.G. wrote the original draft. All authors reviewed and edited the manuscript. I.S.G., J.E.C., and R.H.C. acquired funding. I.S.G., J.E.C., D.J.S., and R.H.C. provided resources. D.J.S., R.H.C., and I.S.G. supervised the work.

DECLARATION OF INTERESTS

S.C.W. and I.S.G. are listed as inventors on antibodies described here. A.R.S. and I.S.G. are co-founders of AbSeek Bio. I.S.G. and A.R.S. are listed as inventors on patent applications for the LIBRA-seq technology. D.J.S. has served as a consultant for AstraZeneca AB. J.E.C. has served as a consultant for Luna Biologics, is a member of the Scientific Advisory Board of Meissa Vaccines, and is founder of IDBiologics. The Crowe laboratory has received funding support in sponsored research agreements from AstraZeneca, IDBiologics, and Takeda. The Georgiev laboratory at VUMC has received unrelated funding from Takeda Pharmaceuticals.

Received: March 24, 2023
Revised: July 17, 2023
Accepted: October 10, 2023
Published: November 6, 2023

REFERENCES

1. Ruf, B.R., and Knuf, M. (2014). The burden of seasonal and pandemic influenza in infants and children. Eur. J. Pediatr. *173*, 265–276. https://doi.org/10.1007/s00431-013-2023-6.
2. Shafagati, N., and Williams, J. (2018). Human metapneumovirus - what we know now. F1000Res. *7*, 135. https://doi.org/10.12688/f1000research.12625.1.
3. Shi, T., McAllister, D.A., O'Brien, K.L., Simoes, E.A.F., Madhi, S.A., Gessner, B.D., Polack, F.P., Balsells, E., Acacio, S., Aguayo, C., et al. (2017). Global, regional, and national disease burden estimates of acute lower respiratory infections due to respiratory syncytial virus in young children in 2015: a systematic review and modelling study. Lancet *390*, 946–958. https://doi.org/10.1016/s0140-6736(17)30938-8.
4. Zimmermann, P., and Curtis, N. (2020). Why is COVID-19 less severe in children? A review of the proposed mechanisms underlying the age-related difference in severity of SARS-CoV-2 infections. Arch. Dis. Child. *106*, 429–439. https://doi.org/10.1136/archdischild-2020-320338.
5. Mehta, N.S., Mytton, O.T., Mullins, E.W.S., Fowler, T.A., Falconer, C.L., Murphy, O.B., Langenberg, C., Jayatunga, W.J.P., Eddy, D.H., and Nguyen-Van-Tam, J.S. (2020). SARS-CoV-2 (COVID-19): What Do We Know About Children? A Systematic Review. Clin. Infect. Dis. *71*, 2469–2479. https://doi.org/10.1093/cid/ciaa556.
6. Chou, J., Thomas, P.G., and Randolph, A.G. (2022). Immunology of SARS-CoV-2 infection in children. Nat. Immunol. *23*, 177–185. https://doi.org/10.1038/s41590-021-01123-9.
7. Mathew, D., Giles, J.R., Baxter, A.E., Oldridge, D.A., Greenplate, A.R., Wu, J.E., Alanio, C., Kuri-Cervantes, L., Pampena, M.B., D'Andrea, K., et al. (2020). Deep immune profiling of COVID-19 patients reveals distinct immunotypes with therapeutic implications. Science *369*, eabc8511. https://doi.org/10.1126/science.abc8511.
8. Kramer, K.J., Wilfong, E.M., Voss, K., Barone, S.M., Shiakolas, A.R., Raju, N., Roe, C.E., Suryadevara, N., Walker, L.M., Wall, S.C., et al. (2022). Single-cell profiling of the antigen-specific response to BNT162b2 SARS-CoV-2 RNA vaccine. Nat. Commun. *13*, 3466. https://doi.org/10.1038/s41467-022-31142-5.
9. Diamond, M.S., and Kanneganti, T.-D. (2022). Innate immunity: the first line of defense against SARS-CoV-2. Nat. Immunol. *23*, 165–176. https://doi.org/10.1038/s41590-021-01091-0.
10. Cromer, D., Steain, M., Reynaldi, A., Schlub, T.E., Wheatley, A.K., Juno, J.A., Kent, S.J., Triccas, J.A., Khoury, D.S., and Davenport, M.P. (2022). Neutralising antibody titres as predictors of protection against SARS-CoV-2 variants and the impact of boosting: a meta-analysis. Lancet. Microbe *3*, e52–e61. https://doi.org/10.1016/s2666-5247(21)00267-6.
11. Krammer, F. (2020). SARS-CoV-2 vaccines in development. Nature *586*, 516–527. https://doi.org/10.1038/s41586-020-2798-3.
12. Wang, Z., Schmidt, F., Weisblum, Y., Muecksch, F., Barnes, C.O., Finkin, S., Schaefer-Babajew, D., Cipolla, M., Gaebler, C., Lieberman, J.A., et al. (2021). mRNA vaccine-elicited antibodies to SARS-CoV-2 and circulating variants. Nature *592*, 616–622. https://doi.org/10.1038/s41586-021-03324-6.
13. Corbett, K.S., Edwards, D.K., Leist, S.R., Abiona, O.M., Boyoglu-Barnum, S., Gillespie, R.A., Himansu, S., Schäfer, A., Ziwawo, C.T., Dipiazza, A.T., et al. (2020). SARS-CoV-2 mRNA vaccine design enabled by prototype pathogen preparedness. Nature *586*, 567–571. https://doi.org/10.1038/s41586-020-2622-0.
14. Khoury, D.S., Cromer, D., Reynaldi, A., Schlub, T.E., Wheatley, A.K., Juno, J.A., Subbarao, K., Kent, S.J., Triccas, J.A., and Davenport, M.P. (2021). Neutralizing antibody levels are highly predictive of immune protection from symptomatic SARS-CoV-2 infection. Nat. Med. *27*, 1205–1211. https://doi.org/10.1038/s41591-021-01377-8.
15. Collier, D.A., Ferreira, I.A.T.M., Kotagiri, P., Datir, R.P., Lim, E.Y., Touizer, E., Meng, B., Abdullahi, A., CITIID-NIHR BioResource COVID-19 Collaboration; and Elmer, A., et al. (2021). Age-related immune response heterogeneity to SARS-CoV-2 vaccine BNT162b2. Nature *596*, 417–422. https://doi.org/10.1038/s41586-021-03739-1.
16. Cele, S., Jackson, L., Khoury, D.S., Khan, K., Moyo-Gwete, T., Tegally, H., San, J.E., Cromer, D., Scheepers, C., Amoako, D.G., et al. (2022). Omicron extensively but incompletely escapes Pfizer BNT162b2 neutralization. Nature *602*, 654–656. https://doi.org/10.1038/s41586-021-04387-1.
17. Barnes, C.O., West, A.P., Huey-Tubman, K.E., Hoffmann, M.A.G., Sharaf, N.G., Hoffman, P.R., Koranda, N., Gristick, H.B., Gaebler, C., Muecksch, F., et al. (2020). Structures of Human Antibodies Bound to SARS-CoV-2 Spike Reveal Common Epitopes and Recurrent Features of Antibodies. Cell *182*, 828–842.e16. https://doi.org/10.1016/j.cell.2020.06.025.
18. Setliff, I., McDonnell, W.J., Raju, N., Bombardi, R.G., Murji, A.A., Scheepers, C., Ziki, R., Mynhardt, C., Shepherd, B.E., Mamchak, A.A., et al. (2018). Multi-Donor Longitudinal Antibody Repertoire Sequencing Reveals the Existence of Public Antibody Clonotypes in HIV-1 Infection. Cell Host Microbe *23*, 845–854.e6. https://doi.org/10.1016/j.chom.2018.05.001.
19. Chen, E.C., Gilchuk, P., Zost, S.J., Suryadevara, N., Winkler, E.S., Cabel, C.R., Binshtein, E., Chen, R.E., Sutton, R.E., Rodriguez, J., et al. (2021). Convergent antibody responses to the SARS-CoV-2 spike protein in convalescent and vaccinated individuals. Cell Rep. *36*, 109604. https://doi.org/10.1016/j.celrep.2021.109604.
20. Tan, T.J.C., Yuan, M., Kuzelka, K., Padron, G.C., Beal, J.R., Chen, X., Wang, Y., Rivera-Cardona, J., Zhu, X., Stadtmueller, B.M., et al. (2021). Sequence signatures of two public antibody clonotypes that bind SARS-CoV-2 receptor binding domain. Nat. Commun. *12*, 3815. https://doi.org/10.1038/s41467-021-24123-7.
21. Zost, S.J., Gilchuk, P., Case, J.B., Binshtein, E., Chen, R.E., Nkolola, J.P., Schäfer, A., Reidy, J.X., Trivette, A., Nargi, R.S., et al. (2020). Potently neutralizing and protective human antibodies against SARS-CoV-2. Nature *584*, 443–449. https://doi.org/10.1038/s41586-020-2548-6.
22. Liu, L., Wang, P., Nair, M.S., Yu, J., Rapp, M., Wang, Q., Luo, Y., Chan, J.F.W., Sahi, V., Figueroa, A., et al. (2020). Potent neutralizing antibodies against multiple epitopes on SARS-CoV-2 spike. Nature *584*, 450–456. https://doi.org/10.1038/s41586-020-2571-7.

23. Pinto, D., Park, Y.J., Beltramello, M., Walls, A.C., Tortorici, M.A., Bianchi, S., Jaconi, S., Culap, K., Zatta, F., De Marco, A., et al. (2020). Cross-neutralization of SARS-CoV-2 by a human monoclonal SARS-CoV antibody. Nature *583*, 290–295. https://doi.org/10.1038/s41586-020-2349-y.

24. Rogers, T.F., Zhao, F., Huang, D., Beutler, N., Burns, A., He, W.T., Limbo, O., Smith, C., Song, G., Woehl, J., et al. (2020). Isolation of potent SARS-CoV-2 neutralizing antibodies and protection from disease in a small animal model. Science *369*, 956–963. https://doi.org/10.1126/science.abc7520.

25. Shi, R., Shan, C., Duan, X., Chen, Z., Liu, P., Song, J., Song, T., Bi, X., Han, C., Wu, L., et al. (2020). A human neutralizing antibody targets the receptor-binding site of SARS-CoV-2. Nature *584*, 120–124. https://doi.org/10.1038/s41586-020-2381-y.

26. Jones, B.E., Brown-Augsburger, P.L., Corbett, K.S., Westendorf, K., Davies, J., Cujec, T.P., Wiethoff, C.M., Blackbourne, J.L., Heinz, B.A., Foster, D., et al. (2020). LY-CoV555, a rapidly isolated potent neutralizing antibody, provides protection in a non-human primate model of SARS-CoV-2 infection. Preprint at bioRxiv. https://doi.org/10.1101/2020.09.30.318972.

27. Hansen, J., Baum, A., Pascal, K.E., Russo, V., Giordano, S., Wloga, E., Fulton, B.O., Yan, Y., Koon, K., Patel, K., et al. (2020). Studies in humanized mice and convalescent humans yield a SARS-CoV-2 antibody cocktail. Science *369*, 1010–1014. https://doi.org/10.1126/science.abd0827.

28. Sun, Y., and Ho, M. (2020). Emerging antibody-based therapeutics against SARS-CoV-2 during the global pandemic. Antib. Ther. *3*, 246–256. https://doi.org/10.1093/abt/tbaa025.37.

29. Weisblum, Y., Schmidt, F., Zhang, F., Dasilva, J., Poston, D., Lorenzi, J.C., Muecksch, F., Rutkowska, M., Hoffmann, H.-H., Michailidis, E., et al. (2020). Escape from neutralizing antibodies by SARS-CoV-2 spike protein variants. Elife *9*, e61312. https://doi.org/10.7554/elife.61312.

30. Chen, R.E., Zhang, X., Case, J.B., Winkler, E.S., Liu, Y., Vanblargan, L.A., Liu, J., Errico, J.M., Xie, X., Suryadevara, N., et al. (2021). Resistance of SARS-CoV-2 variants to neutralization by monoclonal and serum-derived polyclonal antibodies. Nat. Med. *27*, 717–726. https://doi.org/10.1038/s41591-021-01294-w.

31. Wang, P., Nair, M.S., Liu, L., Iketani, S., Luo, Y., Guo, Y., Wang, M., Yu, J., Zhang, B., Kwong, P.D., et al. (2021). Antibody resistance of SARS-CoV-2 variants B.1.351 and B.1.1.7. Nature *593*, 130–135. https://doi.org/10.1038/s41586-021-03398-2.

32. Wang, Q., Guo, Y., Iketani, S., Nair, M.S., Li, Z., Mohri, H., Wang, M., Yu, J., Bowen, A.D., Chang, J.Y., et al. (2022). Antibody evasion by SARS-CoV-2 Omicron subvariants BA.2.12.1, BA.4 and BA.5. Nature *608*, 603–608. https://doi.org/10.1038/s41586-022-05053-w.

33. Wang, Q., Iketani, S., Li, Z., Liu, L., Guo, Y., Huang, Y., Bowen, A.D., Liu, M., Wang, M., Yu, J., et al. (2023). Alarming antibody evasion properties of rising SARS-CoV-2 BQ and XBB subvariants. Cell *186*, 279–286.e8. https://doi.org/10.1016/j.cell.2022.12.018.

34. Sheward, D.J., Kim, C., Fischbach, J., Sato, K., Muschiol, S., Ehling, R.A., Björkström, N.K., Karlsson Hedestam, G.B., Reddy, S.T., Albert, J., et al. (2022). Omicron sublineage BA.2.75.2 exhibits extensive escape from neutralising antibodies. Lancet Infect. Dis. *22*, 1538–1540. https://doi.org/10.1016/s1473-3099(22)00663-6.

35. Cao, Y., Yisimayi, A., Jian, F., Song, W., Xiao, T., Wang, L., Du, S., Wang, J., Li, Q., Chen, X., et al. (2022). BA.2.12.1, BA.4 and BA.5 escape antibodies elicited by Omicron infection. Nature *608*, 593–602. https://doi.org/10.1038/s41586-022-04980-y.

36. Imai, M., Ito, M., Kiso, M., Yamayoshi, S., Uraki, R., Fukushi, S., Watanabe, S., Suzuki, T., Maeda, K., Sakai-Tagawa, Y., et al. (2023). Efficacy of Antiviral Agents against Omicron Subvariants BQ.1.1 and XBB. N. Engl. J. Med. *388*, 89–91. https://doi.org/10.1056/nejmc2214302.

37. Shiakolas, A.R., Kramer, K.J., Johnson, N.V., Wall, S.C., Suryadevara, N., Wrapp, D., Periasamy, S., Pilewski, K.A., Raju, N., Nargi, R., et al. (2022). Efficient discovery of SARS-CoV-2-neutralizing antibodies via B cell receptor sequencing and ligand blocking. Nat. Biotechnol. *40*, 1270–1275. https://doi.org/10.1038/s41587-022-01232-2.

38. Cao, Y., Jian, F., Zhang, Z., Yisimayi, A., Hao, X., Bao, L., Yuan, F., Yu, Y., Du, S., Wang, J., et al. (2022). Rational identification of potent and broad sarbecovirus-neutralizing antibody cocktails from SARS convalescents. Cell Rep. *41*, 111845. https://doi.org/10.1016/j.celrep.2022.111845.

39. Astrazeneca. (2022). AstraZeneca Data on File - REF-173560.

40. Dowell, A.C., Butler, M.S., Jinks, E., Tut, G., Lancaster, T., Sylla, P., Begum, J., Bruton, R., Pearce, H., Verma, K., et al. (2022). Children develop robust and sustained cross-reactive spike-specific immune responses to SARS-CoV-2 infection. Nat. Immunol. *23*, 40–49. https://doi.org/10.1038/s41590-021-01089-8.

41. Fraley, E., Lemaster, C., Banerjee, D., Khanal, S., Selvarangan, R., and Bradley, T. (2021). Cross-reactive antibody immunity against SARS-CoV-2 in children and adults. Cell. Mol. Immunol. *18*, 1826–1828. https://doi.org/10.1038/s41423-021-00700-0.

42. Yang, F., Nielsen, S.C.A., Hoh, R.A., Röltgen, K., Wirz, O.F., Haraguchi, E., Jean, G.H., Lee, J.Y., Pham, T.D., Jackson, K.J.L., et al. (2021). Shared B cell memory to coronaviruses and other pathogens varies in human age groups and tissues. Science *372*, 738–741. https://doi.org/10.1126/science.abf6648.

43. Setliff, I., Shiakolas, A.R., Pilewski, K.A., Murji, A.A., Mapengo, R.E., Janowska, K., Richardson, S., Oosthuysen, C., Raju, N., Ronsard, L., et al. (2019). High-Throughput Mapping of B Cell Receptor Sequences to Antigen Specificity. Cell *179*, 1636–1646.e15. https://doi.org/10.1016/j.cell.2019.11.003.

44. Case, J.B., Rothlauf, P.W., Chen, R.E., Liu, Z., Zhao, H., Kim, A.S., Bloyet, L.M., Zeng, Q., Tahan, S., Droit, L., et al. (2020). Neutralizing Antibody and Soluble ACE2 Inhibition of a Replication-Competent VSV-SARS-CoV-2 and a Clinical Isolate of SARS-CoV-2. Cell Host Microbe *28*, 475–485.e5. https://doi.org/10.1016/j.chom.2020.06.021.

45. Suryadevara, N., Gilchuk, P., Zost, S.J., Mittal, N., Zhao, L.L., Crowe, J.E., Jr., and Carnahan, R.H. (2022). Real-time cell analysis: A high-throughput approach for testing SARS-CoV-2 antibody neutralization and escape. STAR Protoc. *3*, 101387. https://doi.org/10.1016/j.xpro.2022.101387.

46. Zhang, L., Jackson, C.B., Mou, H., Ojha, A., Peng, H., Quinlan, B.D., Rangarajan, E.S., Pan, A., Vanderheiden, A., Suthar, M.S., et al. (2020). SARS-CoV-2 spike-protein D614G mutation increases virion spike density and infectivity. Nat. Commun. *11*, 6013. https://doi.org/10.1038/s41467-020-19808-4.

47. Cao, Y., Jian, F., Wang, J., Yu, Y., Song, W., Yisimayi, A., Wang, J., An, R., Chen, X., Zhang, N., et al. (2023). Imprinted SARS-CoV-2 humoral immunity induces convergent Omicron RBD evolution. Nature *614*, 521–529. https://doi.org/10.1038/s41586-022-05644-7.

48. Kim, S.I., Noh, J., Kim, S., Choi, Y., Yoo, D.K., Lee, Y., Lee, H., Jung, J., Kang, C.K., Song, K.H., et al. (2021). Stereotypic neutralizing V(H) antibodies against SARS-CoV-2 spike protein receptor binding domain in patients with COVID-19 and healthy individuals. Sci. Transl. Med. *13*, eabd6990. https://doi.org/10.1126/scitranslmed.abd6990.

49. Cao, Y., Su, B., Guo, X., Sun, W., Deng, Y., Bao, L., Zhu, Q., Zhang, X., Zheng, Y., Geng, C., et al. (2020). Potent Neutralizing Antibodies against SARS-CoV-2 Identified by High-Throughput Single-Cell Sequencing of Convalescent Patients' B Cells. Cell *182*, 73–84.e16. https://doi.org/10.1016/j.cell.2020.05.025.

50. Raybould, M.I.J., Kovaltsuk, A., Marks, C., and Deane, C.M. (2021). CoV-AbDab: the coronavirus antibody database. Bioinformatics *37*, 734–735. https://doi.org/10.1093/bioinformatics/btaa739.

51. Dong, J., Zost, S.J., Greaney, A.J., Starr, T.N., Dingens, A.S., Chen, E.C., Chen, R.E., Case, J.B., Sutton, R.E., Gilchuk, P., et al. (2021). Genetic and structural basis for SARS-CoV-2 variant neutralization by a two-antibody cocktail. Nat. Microbiol. *6*, 1233–1244. https://doi.org/10.1038/s41564-021-00972-2.

52. Tortorici, M.A., Beltramello, M., Lempp, F.A., Pinto, D., Dang, H.V., Rosen, L.E., McCallum, M., Bowen, J., Minola, A., Jaconi, S., et al. (2020). Ultrapotent human antibodies protect against SARS-CoV-2 challenge via

multiple mechanisms. Science *370*, 950–957. https://doi.org/10.1126/science.abe3354.

53. Wang, Y., Yuan, M., Lv, H., Peng, J., Wilson, I.A., and Wu, N.C. (2022). A large-scale systematic survey reveals recurring molecular features of public antibody responses to SARS-CoV-2. Immunity *55*, 1105–1117.e4. https://doi.org/10.1016/j.immuni.2022.03.019.

54. Westendorf, K., Žentelis, S., Wang, L., Foster, D., Vaillancourt, P., Wiggin, M., Lovett, E., Van Der Lee, R., Hendle, J., Pustilnik, A., et al. (2022). LY-CoV1404 (bebtelovimab) potently neutralizes SARS-CoV-2 variants. Cell Rep. *39*, 110812. https://doi.org/10.1016/j.celrep.2022.110812.

55. Yuan, M., Wang, Y., Lv, H., Tan, T.J.C., Wilson, I.A., and Wu, N.C. (2022). Molecular analysis of a public cross-neutralizing antibody response to SARS-CoV-2. Cell Rep. *41*, 111650. https://doi.org/10.1016/j.celrep.2022.111650.

56. Zhang, Q., Ju, B., Ge, J., Chan, J.F.-W., Cheng, L., Wang, R., Huang, W., Fang, M., Chen, P., Zhou, B., et al. (2021). Potent and protective IGHV3-53/3-66 public antibodies and their shared escape mutant on the spike of SARS-CoV-2. Nat. Commun. *12*, 4210. https://doi.org/10.1038/s41467-021-24514-w.

57. Starr, T.N., Czudnochowski, N., Liu, Z., Zatta, F., Park, Y.-J., Addetia, A., Pinto, D., Beltramello, M., Hernandez, P., Greaney, A.J., et al. (2021). SARS-CoV-2 RBD antibodies that maximize breadth and resistance to escape. Nature *597*, 97–102. https://doi.org/10.1038/s41586-021-03807-6.

58. Kramer, K.J., Johnson, N.V., Shiakolas, A.R., Suryadevara, N., Periasamy, S., Raju, N., Williams, J.K., Wrapp, D., Zost, S.J., Walker, L.M., et al. (2021). Potent neutralization of SARS-CoV-2 variants of concern by an antibody with an uncommon genetic signature and structural mode of spike recognition. Cell Rep. *37*, 109784. https://doi.org/10.1016/j.celrep.2021.109784.

59. Copin, R., Baum, A., Wloga, E., Pascal, K.E., Giordano, S., Fulton, B.O., Zhou, A., Negron, N., Lanza, K., Chan, N., et al. (2021). The monoclonal antibody combination REGEN-COV protects against SARS-CoV-2 mutational escape in preclinical and human studies. Cell *184*, 3949–3961.e11. https://doi.org/10.1016/j.cell.2021.06.002.

60. Alamyar, E., Duroux, P., Lefranc, M.-P., and Giudicelli, V. (2012). IMGT® Tools for the Nucleotide Analysis of Immunoglobulin (IG) and T Cell Receptor (TR) V-(D)-J Repertoires, Polymorphisms, and IG Mutations: IMGT/V-QUEST and IMGT/HighV-QUEST for NGS (Humana Press), pp. 569–604. https://doi.org/10.1007/978-1-61779-842-9_32.

61. Gupta, N.T., Vander Heiden, J.A., Uduman, M., Gadala-Maria, D., Yaari, G., and Kleinstein, S.H. (2015). Change-O: a toolkit for analyzing large-scale B cell immunoglobulin repertoire sequencing data. Bioinformatics *31*, 3356–3358. https://doi.org/10.1093/bioinformatics/btv359.

62. Punjani, A., Rubinstein, J.L., Fleet, D.J., and Brubaker, M.A. (2017). cryoSPARC: algorithms for rapid unsupervised cryo-EM structure determination. Nat. Methods *14*, 290–296. https://doi.org/10.1038/nmeth.4169.

63. Pettersen, E.F., Goddard, T.D., Huang, C.C., Meng, E.C., Couch, G.S., Croll, T.I., Morris, J.H., and Ferrin, T.E. (2021). scp>UCSF ChimeraX</scp> : Structure visualization for researchers, educators, and developers. Protein Sci. *30*, 70–82. https://doi.org/10.1002/pro.3943.

64. Vlasova, A.N., Diaz, A., Damtie, D., Xiu, L., Toh, T.H., Lee, J.S.Y., Saif, L.J., and Gray, G.C. (2022). Novel Canine Coronavirus Isolated from a Hospitalized Patient With Pneumonia in East Malaysia. Clin. Infect. Dis. *74*, 446–454. https://doi.org/10.1093/cid/ciab456.

65. Georgiev, I.S., Joyce, M.G., Yang, Y., Sastry, M., Zhang, B., Baxa, U., Chen, R.E., Druz, A., Lees, C.R., Narpala, S., et al. (2015). Single-Chain Soluble BG505.SOSIP gp140 Trimers as Structural and Antigenic Mimics of Mature Closed HIV-1 Env. J. Virol. *89*, 5318–5329. https://doi.org/10.1128/jvi.03451-14.

66. Crawford, K.H.D., Eguia, R., Dingens, A.S., Loes, A.N., Malone, K.D., Wolf, C.R., Chu, H.Y., Tortorici, M.A., Veesler, D., Murphy, M., et al. (2020). Protocol and Reagents for Pseudotyping Lentiviral Particles with SARS-CoV-2 Spike Protein for Neutralization Assays. Viruses *12*, 513. https://doi.org/10.3390/v12050513.

67. Kaas, Q., Ruiz, M., and Lefranc, M.P. (2004). IMGT/3Dstructure-DB and IMGT/StructuralQuery, a database and a tool for immunoglobulin, T cell receptor and MHC structural data. Nucleic Acids Res. *32*, D208–D210. https://doi.org/10.1093/nar/gkh042.

68. Ohi, M., Li, Y., Cheng, Y., and Walz, T. (2004). Negative staining and image classification — powerful tools in modern electron microscopy. Biol. Proced. Online *6*, 23–34. https://doi.org/10.1251/bpo70.

69. Mastronarde, D.N. (2003). SerialEM: A Program for Automated Tilt Series Acquisition on Tecnai Microscopes Using Prediction of Specimen Position. Microsc. Microanal. *9*, 1182–1183. https://doi.org/10.1017/s1431927603445911.

STAR★METHODS

KEY RESOURCES TABLE

REAGENT or RESOURCE	SOURCE	IDENTIFIER
Antibodies		
APC-Cy7 Mouse Anti-Human CD14	BD	Cat# 561709; RRID: AB_10893806
FITC Anti-Human CD3 (OKT3)	Tonbo Biosciences	Cat# 35–0037; RRID: AB_2621662
BV711 Mouse Anti-Human CD19	BD	Cat# 563036; RRID: AB_2737968
PE-Cy5 Mouse Anti-Human IgG	BD	Cat# 551497; RRID: AB_394220
Goat anti-human IgG antibody (peroxidase)	Jackson ImmunoResearch	Cat#109-035-088, RRID:AB_2337584
Anti-Mouse IgG HRP Conjugate	Promega	Cat#W4021
Monoclonal anti-influenza 3602-1707	Setliff et al.[43]	N/A
Monoclonal anti-SARS-CoV-2 NTD 5317-9	Shiakolas et al.[37]	N/A
Monoclonal anti-SARS-CoV-2 71281-3	This paper	GenBank: OR486977, OR486978
Monoclonal anti-SARS-CoV-2 71281-6	This paper	GenBank: OR486983, OR486984
Monoclonal anti-SARS-CoV-2 71281-20	This paper	GenBank: OR487011, OR487012
Monoclonal anti-SARS-CoV-2 71281-22	This paper	GenBank: OR487015, OR487016
Monoclonal anti-SARS-CoV-2 71281-26	This paper	GenBank: OR487023, OR487024
Monoclonal anti-SARS-CoV-2 71281-31	This paper	GenBank: OR487033, OR487034
Monoclonal anti-SARS-CoV-2 71281-32	This paper	GenBank: OR487035, OR487036
Monoclonal anti-SARS-CoV-2 71281-33	This paper	GenBank: OR487037, OR487038
Monoclonal anti-SARS-CoV-2 71281-35	This paper	GenBank: OR487041, OR487042
Monoclonal anti-SARS-CoV-2 71281-36	This paper	GenBank: OR487043, OR487044
Monoclonal anti-SARS-CoV-2 71281-37	This paper	GenBank: OR487045, OR487046
Monoclonal anti-SARS-CoV-2 71282-4	This paper	GenBank: OR487057, OR487058
Monoclonal anti-SARS-CoV-2 71282-6	This paper	GenBank: OR487061, OR487062
Monoclonal anti-SARS-CoV-2 71282-7	This paper	GenBank: OR487063, OR487064
Monoclonal anti-SARS-CoV-2 71282-10	This paper	GenBank: OR487069, OR487070
Monoclonal anti-SARS-CoV-2 71282-14	This paper	GenBank: OR487077, OR487078
Monoclonal anti-SARS-CoV-2 71282-18	This paper	GenBank: OR487085, OR487086
LY-CoV1404	Westendorf et al.[54]	N/A
REGN10987	Copin et al.[59]	N/A
2–7	Liu et al.[22]	N/A
CR3022	Yuan et al.[55]	N/A
CB6	Shi et al.[25]	N/A
DENV-2D22	James Crowe Jr.	N/A
Bacterial and virus strains		
VSV-SARS-CoV-2	Case et al.[44]	N/A
VSV-SARS-CoV	This paper	N/A
SARS-CoV-2 D614G pseudotyped lentivirus	Sheward et al.[34]	N/A
SARS-CoV-2 BA.2 pseudotyped lentivirus	Daniel Sheward	N/A
SARS-CoV-2 BA.5 pseudotyped lentivirus	Sheward et al.[34]	N/A
SARS-CoV-2 BA.4.6 pseudotyped lentivirus	Sheward et al.[34]	N/A
SARS-CoV-2 BA.2.75.2 pseudotyped lentivirus	Sheward et al.[34]	N/A
SARS-CoV-2 XBB pseudotyped lentivirus	Daniel Sheward	N/A
SARS-CoV-2 BQ.1.1 pseudotyped lentivirus	Daniel Sheward	N/A
SARS-CoV-2 XBB.1.5 pseudotyped lentivirus	Daniel Sheward	N/A
SARS-CoV-2 BA.2.75 + R346T pseudotyped lentivirus	This paper	N/A

(*Continued on next page*)

Continued

REAGENT or RESOURCE	SOURCE	IDENTIFIER
Biological samples		
PBMCs from donors	Mary Arildsen	N/A
Chemicals, peptides, and recombinant proteins		
Ghost dye red 780	Tonbo biosciences	Cat#13-0865
Live/Dead fixable aqua dead cell stain kit	Thermo Fisher Scientific	Cat#L34957
Streptavidin HRP	Thermo Fisher Scientific	Cat#ENN100
Polyethyleniminine Linear MW 25000	Polysciences	Cat#23966-1
1-Step Ultra TMB-ELISA Substrate Solution	Thermo Fisher Scientific	Cat#34029
ACE2 with mouse Fc	Sino Biological	Cat#10108-H05H-100
Streptavidin R-phycoerythrin (SA-PE)	Invitrogen	Cat#S866
Galanthus nivalis lectin	Vector Laboratories	Cat#AL-1243-5
Protein A resin	GenScript	Cat#L00210
SARS-CoV-2 S1	Sino Biological	Cat#40591-V08H
SARS-CoV-2 S2	Sino Biological	Cat#40590-V08B
SARS-CoV-2 RBD	Sino Biological	Cat#40592-VNAH
SARS-CoV-2 NTD	Sino Biological	Cat#40591-V49H
HCoV-229E S	Sino Biological	Cat#40605-V08B
HCoV-NL63 S	Sino Biological	Cat#40604-V08B
SARS-CoV-2 S (Hexapro)	PMID: 32703906	N/A
SARS-CoV S (S-2P)	PMID: 28807998	N/A
HCoV-OC43 S (S-2P)	McLellan Lab	N/A
HCoV-HKU1 S (S-2P)	PMID: 28807998	N/A
MERS-CoV S (S-2P)	PMID: 28807998	N/A
A/New Caledonia/20/99 (H1N1)	Barney Graham	GenBank: ACF41878
BG505.N332T.SOSIP.664 gp140 trimer	Ivelin Georgiev	N/A
SARS-CoV-2 S (Hexapro Alpha)	This paper	N/A
SARS-CoV-2 S (Hexapro Beta)	This paper	N/A
SARS-CoV-2 S (Hexapro Delta)	This paper	N/A
SARS-CoV-2 S (Hexapro Omicron BA.1)	This paper	N/A
SARS-CoV-2 S (Hexapro Omicron BA.2)	This paper	N/A
SARS-CoV-2 S (Omicron BA.4/5)	Sino Biological	Cat#40589-V08H32
LYRa11 S (S-2P)	This paper	N/A
RaTG13 S (S-2P)	This paper	N/A
Civet-007-2004 S (S-2P)	This paper	N/A
Critical commercial assays		
EZ link Sulfo-NHS-LC-biotin	Thermo Fisher Scientific	Cat#21327
Solulink protein-oligonucleotide conjugation kit	TriLink Biotechnologies	Cat#S-9011
B cell Single Cell V(D)J solution	10X Genomics	N/A
ExpiFectamine™ 293 Transfection Kit	Thermo Fisher Scientific	Cat#A14526
StrepTrap XT prepacked chromatography column	Cytiva	Cat#29401322
Deposited data		
71281 heavy and light chain sequences	This paper	GenBank: OR486973-OR487050
71282 heavy and light chain sequences	This paper	GenBank: OR487051-OR487090
Raw next-generation sequencing data	This paper	SRA: PRJNA1014462
71281-33 Fab nsEM map data	This paper	EMDB: EMD-41075, EMD-41076
Experimental models: Cell lines		
Human: Expi293F cells	Thermo Fisher Scientific	Cat#A14527
ExpiCHO cells	Thermo Fisher Scientific	Cat#A29127

(*Continued on next page*)

Continued

REAGENT or RESOURCE	SOURCE	IDENTIFIER
Vero E6 cells	ATCC	Cat#CRL-1586
HEK-293T-hACE2 cells	BEI	Cat#NR-52511
HEK-293T/17 cells	ATCC	Cat#CRL-11268
HEK-293T cells	ATCC	Cat#CRL-3216
Oligonucleotides		
Oligonucleotides for protein DNA-barcoding	Setliff et al.[43]	N/A
Software and algorithms		
Flowjo v10	TreeStar	https://www.flowjo.com/
GraphPad Prism 9.5.0	https://www.graphpad.com:443/	N/A
Cell Ranger	10X Genomics	https://support.10xgenomics.com/single-cell-gene-expression/software/downloads/latest
HighV-Quest	Alamyar et al.[60]	http://www.imgt.org/IMGTindex/IMGTHighVQUEST.php
ChangeO	Gupta et al.[61]	https://changeo.readthedocs.io/en/stable/
cryoSPARC	Punjani et al.[62]	https://cryosparc.com/updates
ChimeraX	Petterson et al.[63]	https://www.cgl.ucsf.edu/chimerax/download.html

RESOURCE AVAILABILITY

Lead contact

Further information and requests for resources and reagents should be directed to the lead contact, Ivelin Georgiev (ivelin.georgiev@vanderbilt.edu).

Materials availability

All unique/stable reagents generated in this study are available from the lead contact with a completed Materials Transfer Agreement. Please direct resource and reagent requests to the lead contact specified above, Ivelin Georgiev.

Data and code availability

- Sequences for antibodies identified and characterized in this study have been deposited to GenBank under GenBank accession numbers Genbank: OR486973-OR487050 (for 71281 antibodies) and Genbank: OR487051-OR487090 (for 71282 antibodies). Raw sequencing data used in this study are available on the Sequence Read Archive under BioProject accession number SRA: PRJNA1014462. nsEM map data of Fab 71281–33 in complex with SARS-CoV-2 spike is available on the Electron Microscopy Databank under accession numbers EMDB: EMD-41075 and EMDB: EMD-41076.
- This paper does not report original code.
- Any additional information required to reanalyze the data reported in this paper is available from the lead contact upon request.

EXPERIMENTAL MODELS AND SUBJECT DETAILS

Human subjects

All research in this study complies with relevant ethical regulations. Vanderbilt University Medical Center Institutional Review Board approval was obtained (VUMC #210733). All donors were children between the ages of 5 months and 18 years old. Blood samples were collected with consent on June 24th and August 18th of 2021 and then PBMCs were isolated upon receipt. PBMCs were pooled into either group 71281 (no known history of SARS-CoV-2 infection or vaccination) or group 71282 (known history of infection or vaccination) based on self-reporting. Additional details on the age and gender distribution of both groups is further detailed in Figure S1. Additional information about these donors is unavailable.

Cell lines

A variety of cell lines were used for different assays in this study. Expi293F mammalian cells (ThermoFisher, A14527) were maintained in FreeStyle F17 expression medium supplemented with a final concentration of 0.1% Pluronic Acid F-68 and 4mM L-Glutamine. ExpiCHO cells (ThermoFisher, A29127) were maintained in ExpiCHO Expression medium(ThermoFisher, A2910002). Cells were cultured at 37 C with 8% CO_2 saturation while shaking. Vero E6 cells (ATCC, CRL-1586) and all HEK293T cell lines (ATCC, CRL-3216; ATCC, CRL-11268; BEI, NR-52511) were maintained in Dulbecco's minimal essential medium (DMEM) supplemented

with 10mM HEPES pH 7.3, 1X non-essential amino acids, 1mM sodium pyruvate, 100U/mL of penicillin-streptomycin, and 10% fetal bovine serum and grown in 37 C with 5% CO_2. Authentication analysis was not performed on the cell lines used.

Viruses

The generation of a replication-competent VSV expressing SARS-CoV-2 S protein with a 21 amino acid C-terminal deletion that replaces the VSV G protein (VSV-SARS-CoV-2) was described previously (Case et al., 2020b). The S protein-expressing VSV virus was propagated in MA104 cell culture monolayers (African green monkey, ATCC CRL-2378.1) as described previously (Case et al., 2020b), and viral stocks were titrated on Vero E6 cell monolayer cultures. VSV plaques were visualized using neutral red staining. All work with infectious SARS-CoV-2 was performed in Institutional Biosafety Committee approved BSL3 and A-BSL3 facilities at Washington University School of Medicine using appropriate positive pressure air respirators and protective equipment.

METHOD DETAILS

Blood sample collection and preparation

Blood was collected for diagnostic testing into K2EDTA-coated Becton-Dickenson tubes and mixed to prevent coagulation. Blood was refrigerated after routine hematology testing was performed, until selection for the study (within 48 h). Blood samples were selected and delivered to the Georgiev lab and PBMCs were isolated immediately upon receipt. Use of the leftover diagnostic peripheral blood samples is covered by Vanderbilt University Medical Center IRB approval (#210733).

PBMC isolation

Upon receiving samples from VUMC Diagnostic Laboratories, whole blood was separated and pooled based on the parameters described in the results section. Pooled blood samples were diluted with 3 parts DPBS. 12.5 mL of Ficoll was added to 50 mL conical tubes and then the diluted blood (up to 30mL per 50 mL conical) was pipetted to mix before carefully layering it on top of the Ficoll. Without disrupting the Ficoll/Blood interface, tubes were centrifuged at 400 g for 30 min. The buffy coat was carefully removed and transferred to a new 50 mL conical up to a maximum of 25 mL per tube. Tubes were then topped to the 50 mL mark with DPBS and inverted to mix. Tubes were again centrifuged at 400 g. For each tube, the pellets were resuspended in ACK lysing buffer and incubated for 1 min at room temperature. Resuspended pellets from the same pooled samples were combined and then cells were counted. Tubes were filled up to 50 mL with DPBS and centrifuged at 200 g for 5 min at room temperature. Supernatants were decanted and pellets were resuspended in CryoStor Freeze Media in aliquots of 1 mL each between 10 and 100 million cells/mL. Isolated PBMCs were subject to slow freezing and then placed into liquid nitrogen for storage.

Some PBMCs were isolated using the EasySep Direct Human PBMC Isolation Kit (Stemcell) according to kit instructions. In short, EDTA was added to pooled blood samples, mixed with the isolation cocktail, and incubated. RapidSpheres were then added to the sample and mixed, followed by incubation of the tube inside of the "The Big Easy" magnet (Cat# 18001). The enriched cell suspension was then poured into a new tube, followed by mixing with more RapidSpheres. Cell mixture was incubated in the magnet for a 2nd time for additional separation. The enriched cell suspension was poured into a new tube and the process was repeated for a third time. Isolated cells were poured into a new tube and subsequently counted and frozen for use as detailed above.

Antigen expression and purification

An assortment of recombinant soluble protein antigens was used in the LIBRA-seq experiment and assays. All Expi293F cells were cultured at 8% CO_2 saturation and 37°C with shaking in FreeStyle F17 expression media (Thermo Fisher) supplemented to a final concentration of 0.1% Pluronic Acid F-68 and 4 mM L-glutamine.

Plasmids were transiently transfected in Expi293F cells using polyethylenimine or ExpiFectamine transfection reagent (Thermo Fisher Scientific) and encoded the following: residues 1–1208 of the SARS-CoV-2 spike with a mutated S1/S2 cleavage site, proline substitutions at positions 817, 892, 899, 942, 986 and 987, and a C-terminal T4-fibritin trimerization motif, an 8x HisTag, and a TwinStrepTag (SARS-CoV-2 S Hexapro (HP)); 1–1208 of the SARS-CoV-2 spike with a mutated S1/S2 cleavage site, proline substitutions at positions 817, 892, 899, 942, 986 and 987, as well as mutations L18F, D80A, L242-244L del, R246I, K417N, E484K, N501Y, and a C-terminal T4-fibritin trimerization motif, an 8x HisTag, and a TwinStrepTag (SARS-CoV-2 spike HP Beta); 1–1208 of the SARS-CoV-2 spike with a mutated S1/S2 cleavage site, proline substitutions at positions 817, 892, 899, 942, 986 and 987, as well as mutations 69-70del, Y144del, N501Y, A570D, P681H, and a C-terminal T4-fibritin trimerization motif, an 8x HisTag, and a TwinStrepTag (SARS-CoV-2 spike HP Alpha); residues 1–1190 of the SARS-CoV spike with proline substitutions at positions 968 and 969, and a C-terminal T4-fibritin trimerization motif, an 8x HisTag, and a TwinStrepTag (SARS-CoV S-2P); residues 1–1291 of the MERS-CoV spike with a mutated S1/S2 cleavage site, proline substitutions at positions 1060 and 1061, and a C-terminal T4-fibritin trimerization motif, an AviTag, an 8x HisTag, and a TwinStrepTag (MERS-CoV S-2P Avi); residues 1–1278 of the HCoV-OC43 spike with proline substitutions at positions 1070 and 1071, and a C-terminal T4-fibritin trimerization motif, an 8x HisTag, and a TwinStrepTag (HCoV-OC43 S-2P); residues 1–1277 of the HCoV-HKU1 spike with a mutated S1/S2 cleavage site, proline substitutions at positions 1067 and 1068, and a C-terminal T4-fibritin trimerization motif, an 8x HisTag, and a TwinStrepTag (HCoV-HKU1 S-2P); 1–1208 of the SARS-CoV-2 spike with a mutated S1/S2 cleavage site, proline substitutions at positions 817, 892, 899, 942, 986 and 987, as well as mutations T19R, del157/158, L452R, T478K, D614G, P681R, D950N, and a C-terminal T4-fibritin

trimerization motif, Avitag, HRV3C, 8x HisTag, and a TwinStrepTag (SARS-CoV-2 Delta S HP); 1–1208 of the SARS-CoV-2 spike with a mutated S1/S2 cleavage site, proline substitutions at positions 817, 892, 899, 942, 986 and 987, as well as mutations A67V, del69/70, T95I, G142D, del143/145, del11, L212I, G339D, S371L, S373P, S375F, S477N, T478K, E484A, Q493R, Q496S, Q498R, N501Y, Y505H, T547K, D614G, H655Y, N679K, P681H, N764K, D796Y, N856K, Q954H, N969K, L981F, and a C-terminal T4-fibritin trimerization motif, Avitag, HRV3C, 8x HisTag, and a TwinStrepTag (SARS-CoV-2 Omicron BA.1 S HP); 1–1208 of the SARS-CoV-2 spike with a mutated S1/S2 cleavage site, proline substitutions at positions 817, 892, 899, 942, 986 and 987, as well as mutations T19I, Del24-26, G142D, V213G, G339D, S371F, S373P, S375F, T376A, D405N, R408S, K417N, N440K, S477N, T478K, E484A, Q493R, Q498R, N501Y, Y505H, D614G, H655Y, N679K, P681H, N764K, D796Y, Q954H, N969K, and a C-terminal T4-fibritin trimerization motif, Avitag, HRV3C, 8x HisTag, and a TwinStrepTag (SARS-CoV-2 Omicron BA.2 S HP); 1–1204 of the RaTG13 spike (ENA QHR63300.2) with proline substitutions at positions 982 and 983, and a C-terminal T4-fibritin trimerization motif, Avitag, HRV3C, 8x HisTag, and a TwinStrepTag (RaTG13 S-2P); 1–1194 of the LYRa11 (ENA AHX37558.1) spike with proline substitutions at positions 972 and 973, and a C-terminal T4-fibritin trimerization motif, Avitag, HRV3C, 8x HisTag, and a TwinStrepTag (LYRa11 S-2P); 1–1190 of the Civet-007/2004 spike (ENA AAU04646.1) with proline substitutions at positions 968 and 969, and a C-terminal T4-fibritin trimerization motif, Avitag, HRV3C, 8x HisTag, and a TwinStrepTag (Civet-007-2004 S-2P); 1–1387 of the CCoV-HuPn-2018 spike[64] with proline substitutions at positions 1140 and 1141, and a C-terminal T4-fibritin trimerization motif, Avitag, HRV3C, 8x HisTag, and a TwinStrepTag (CCoV-HuPn-2018 S-2P). All coronavirus spike supernatants were collected 5–7 days post transfection, sterile filtered, and purified over a StrepTrap XT column (Cytiva Life Sciences). Purified proteins were further purified using a size exclusion Superose6 Increase column (Cytiva Life Sciences). For LIBRA-seq, the purified antigens were then biotinylated with the EZ-Link Sulfo-NHS-Biotin (Thermo Fisher Scientific) using a 50:1 biotin to protein molar ratio for calculations.

Recombinant HIV-1 gp140 SOSIP BG505 N332T trimer[65] was cultured in Expi293F cells and transfected in the same method as above. The clarified supernatant was run over an affinity column of agarose-bound *Galanthus nivalis* lectin (GNA, Snowdrop) slowly at 4°C. The column was washed with 1X PBS and bound protein was eluted with 1M methyl-a-D-mannopyranoside in PBS. The protein eluate was buffer exchanged into 1X PBS and then purified by size exclusion chromatography using a Superdex 200 Increase 10/300 GL Sizing column on the AKTA FPLC system (GE Life Sciences). The fractions of purified protein were analyzed by SDS-PAGE and binding was confirmed using ELISA with known antibodies.

The recombinant HA protein (A/New Caledonia/20/99 H1N1 GenBank ACF41878 (NC99)) was produced using Expi 293F cells and the Expifectamine 293 transfection reagent. The protein contains the HA ectodomain with a point mutation at the sialic acid-binding site (Y98F), T4 fibritin foldon trimerization domain, AviTag, and hexahistidine-tag. The cells were cultured for 4–5 days, then the supernatant was harvested and sterile filtered. The pH and NaCl concentration were adjusted by adding 1M Tris-HCl (pH 7.5) and 5M NaCl to 50 mM and 500 mM, respectively. The supernatant was then mixed with Ni Sepharose excel resin (GE Healthcare) to capture the hexahistidine tag. The resin was isolated in a column by gravity and the captured HA protein was eluted by a Tris-NaCl (pH 7.5) buffer containing 300 mM imidazole. The eluted protein was further purified by size exclusion chromatography using a HiLoad 16/60 Superdex 200 column (GE Healthcare). Fractions containing the appropriate sized HA protein were concentrated, analyzed by SDS-PAGE, and tested for antigenicity by ELISA using known antibodies. The proteins were then stored at −80C until use.

The SARS-CoV-2 S1, SARS-CoV-2 S2, SARS-CoV-2 RBD, and SARS-CoV-2 NTD subdomains as well as recombinant SARS-CoV-2 Omicron BA.4/5 S HP, and HCoV-229E S were purchased from Sino Biological.

Oligonucleotide barcodes

We used oligonucleotides composed of a 15 bp antigen barcode, a sequence designed for annealing to the template switch oligo on the 10X bead-delivered oligos, and contains truncated TruSeq small RNA read 1 sequences in the following structure: 5′-CCTTGGCACCCGAGAATTCCANNNNNNNNNNNNNCCCATATAAGA*A*A-3′, where Ns represent the antigen barcode. For each antigen we used the following barcode sequences: SARS-CoV-2 S HP (ACAATTTGTCTGCGA), SARS-CoV-2 Alpha S HP (GGTAGCCCTAGAGTA), SARS-CoV-2 Beta S HP (ATTCGCCTTACGCAA), SARS-CoV S-2P (GACCTCATTGTGAAT), LYRa11 S-2P (AGACTAATAGCTGAC), RaTG13 S-2P (TGTGTATTCCCTTGT), Civet-007-2004 S-2P (GACAAGTGATCTGCA), MERS S-2P (AACCTTCCGTCTAAG), HCoV-OC43 S-2P (TAACTCAGGGCCTAT), HCoV-HKU1-S-2P (CAGCCCACTGCAATA), HCoV-229E S (TACGCCTATAACTTG), BG505 gp140 SOSIP N332T (AACCCACCGTTGTTA), HA NC99 (GCTCCTTTACACGTA). Oligos were ordered from Sigma-Aldrich and IDT with a 5′ amino modification and HPLC purified.

Labeling antigens with DNA oligonucleotide barcodes

For each antigen described above, the unique DNA barcodes were directly conjugated to the antigen using a SoluLINK Protein-Oligonucleotide Conjugation kit (TriLink, S-9011) according to kit protocol. In short, we desalted the oligonucleotide and protein, modified the amino-oligonucleotide with the 4FB cross-linker, and modified the biotinylated antigen with S-HyNic. Afterward, the 4FB-oligonucleotide and the HyNic-antigen were mixed to form a stable bond between the protein and the oligonucleotide. The antigen-oligonucleotide concentrations were then determined using a bicinchoninic acid (BCA) assay, and the HyNic molar substitution ratios of each antigen-oligonucleotide conjugate was determined using a NanoDrop according to SoluLINK protocol instructions. Excess oligonucleotide was removed from the protein-oligonucleotide conjugates using an AKTA FPLC and were subsequently verified using SDS-PAGE and silver stain. The optimal amounts of antigen-oligonucleotide conjugates to be used in antigen-specific B cell sorting were then determined through flow cytometry titration experiments on cell lines expressing BCRs of known specificities.

Antigen specific B cell sorting

To start, PBMCs were thawed, washed, and counted. Viability was evaluated using Trypan Blue. The cells were then washed with a solution of DPBS supplemented with 0.1% Bovine serum albumin (BSA). Afterward, the cells were resuspended in DPBS-BSA and stained with cell markers: Ghost Red 780 for viability, CD14-APC-Cy7, CD3-FITC, CD19-BV711 and IgG-PE-Cy5. Additionally, antigen-oligo conjugates were added to the stain. After a 30-min incubation in the dark at room temperature, the cells were washed again three times with DPBS-BSA at 300 g for 5 min. Then, the cells were incubated for 15 min at room temperature with Streptavidin-PE to label cells with bound antigen. The cells were again washed three times with DPBS-BSA, resuspended in DPBS, and sorted by FACS. Antigen positive B cells were bulk sorted and delivered to the Vanderbilt Technologies for Advanced Genomics (VANTAGE) sequencing core at an appropriate target concentration for 10X Genomics library preparation and subsequent sequencing. FACS data were analyzed using FlowJo.

Sample and library preparation for sequencing

Single-cell suspensions were processed using the Chromium Controller microfluidics device (10X Genomics) and the B cell Single Cell V(D)J solution as per the manufacturer's instructions. The aim was to capture 10,000 B cells per 1/8 10X cassette. Slight modifications were made to intercept, amplify, and purify the antigen barcode libraries, as previously described.[43]

Sequence processing and bioinformatics analysis

Our established pipeline was followed, which takes paired-end FASTQ files of oligonucleotide libraries as input, to process and annotate reads for cell barcodes, unique molecular identifiers (UMIs) and antigen barcodes, resulting in a cell barcode-antigen barcode UMI count matrix.[43] B cell receptor contigs were processed using CellRanger (10x Genomics) and GRCh38 as reference, while the antigen barcode libraries were also processed using CellRanger (10x Genomics). The cell barcodes that overlapped between the two libraries formed the basis of the subsequent analysis. Cell barcodes that had only non-functional heavy chain sequences as well as cells with multiple functional heavy chain sequences and/or multiple functional light chain sequences, were eliminated, reasoning that these may be multiplets. We also aligned the B cell receptor contigs (filtered_contigs.fasta file output by CellRanger, 10x Genomics) to IMGT reference genes using HighV-Quest.[60] The output of HighV-Quest was parsed using ChangeO,[61] and combined with an antigen barcode UMI count matrix. Finally, we determined the LIBRA-seq score for each antigen in the library for every cell as previously described.[43]

High-throughput antibody microscale expression and purification

For high-throughput production of recombinant antibodies, a microscale approach was employed. For antibody expression, microscale transfection was performed (~1 mL per antibody) with CHO cell cultures using the Gibco ExpiCHO Expression System and a protocol for deep 96-well blocks (Thermo Fisher Scientific). Briefly, synthesized antibody-encoding DNA (~2 μg per transfection) was added to OptiPro serum-free medium (OptiPro SFM), incubated with ExpiFectamine CHO Reagent, and added to 800 μL of ExpiCHO cell cultures in deep 96-well blocks using a ViaFlo384 liquid handler (Integra Biosciences). The plates were incubated on an orbital shaker at 1,000 r.p.m. with an orbital diameter of 3 mm at 37°C in 8% CO2. The next day after transfection, ExpiFectamine CHO Enhancer and ExpiCHO Feed reagents (Thermo Fisher Scientific) were added to the cells, followed by 4 more days of incubation. Culture supernatants were collected after centrifuging the blocks at 450 g for 5 min and were stored at 4°C until use. For high-throughput microscale antibody purification, fritted deep-well plates were used containing 25 μL of settled Protein G resin (GE Healthcare Life Sciences) per well. Clarified culture supernatants were incubated with protein G resin for antibody capturing, washed with PBS using a 96-well plate manifold base (Qiagen) connected to the vacuum and eluted into 96-well PCR plates using 86 μL of 0.1 M glycine-HCl buffer, pH 2.7. Purified antibodies were then neutralized with 14 μL of 1 M Tris-HCl pH 8.0 and buffer exchanged into PBS using Zeba Spin Desalting plates (Thermo Fisher Scientific). Purified antibodies were then stored at 4°C until use.

Antibody expression and purification

Variable heavy and light genes were inserted into custom plasmids that encode the constant region for the human IgG1 heavy chain and respective lambda and kappa light chains (pTwist CMV BetaGlobin WPRE *Neo* vector, Twist Bioscience). The antibodies were expressed in Expi293F cells by co-transfecting heavy chain and light chain expressing plasmids using polyethylenimine or Expifectamine transfection reagent, and the cells were cultured for 4–5 days. These cells were maintained as previously described in the antigen purification methods. Cultures were harvested, centrifuged and supernatant was 0.45 μm filtered with Nalgene Rapid Flow Disposable Filter Units with PES membrane. The filtered supernatant was run over a column containing Protein A agarose resin that was equilibrated with PBS. The column was washed with PBS, and then the antibodies were eluted with 100mM Glycine HCl at 2.7 pH directly into a 1:10 volume of 1M Tris-HCl pH 8.0. Eluted antibodies were buffer exchanged into PBS using using Amicon Ultra centrifugal filter units, centrifuging and topping off three times with PBS, and finally concentrated. The antibodies were analyzed by SDS-PAGE. Antibody plasmids were sequenced to confirm the expected heavy and light chain match.

ELISA

To evaluate the binding of the expressed antibodies, soluble purified antigen was plated at a concentration of 2 μg/mL and incubated overnight at 4°C. The next day, the plates were washed three times with a PBS solution containing 0.05% Tween 20 (PBS-T) and then

coated with 5% milk powder in PBS-T. The plates were incubated for 1 h at room temperature and then washed three times with PBS-T. The primary antibodies were diluted in 1% milk in PBS-T, starting at a concentration of 10 μg/mL with a serial 1:5 or 1:10 dilution and then added to the plate. The plates were incubated for an additional hour at room temperature and then washed three times with PBS-T. The secondary antibody, goat anti-human IgG conjugated to peroxidase, was added at a dilution of 1:10,000 in 1% milk in PBS-T to the plates, which were incubated for 1 h at room temperature. The plates were washed three times with PBS-T and then developed by adding TMB substrate to the plates. The plates were incubated for 10 min at room temperature, and the reaction was stopped with 1N sulfuric acid. Plates were read at 450 nm. The data is shown as one representative biological replicate with the mean ± SEM for one ELISA experiment. The ELISAs were repeated 2 or more times. The area under the curve (AUC) was calculated using GraphPad Prism 9.5.0.

ACE2 competition ELISA

96-well plates were coated with 2 μg/mL of purified recombinant SARS-CoV-2 spike protein, and left to incubate overnight at 4°C. The following day, the plates were washed three times with a PBS solution containing 0.05% Tween 20 (PBS-T) and then coated with 5% nonfat dry milk in PBS-T. The plates were incubated for 1 h at room temperature and then washed three times with PBS-T. Next, purified antibodies were diluted in 1% nonfat dry milk in PBS-T at a concentration of 10 μg/mL and added to the wells in triplicate, followed by incubation for an additional hour at room temperature. Without washing, recombinant human ACE2 protein with a mouse Fc tag was added to the wells for a final concentration of 0.4 μg/mL of ACE2 and incubated for 40 min at room temperature. The plates were washed three times with PBS-T and bound ACE2 was detected using HRP-conjugated anti-mouse Fc antibody and TMB substrate. The plates were incubated for 10 min at room temperature, and then the reaction was stopped with 1N sulfuric acid. Plates were read at 450 nm ACE2 binding without antibody served as a control. The experiment was done in biological replicate and technical triplicates.

Antibody competition ELISA

Antibody competition ELISAs were performed similarly to the regular binding ELISA protocol described above, with some alterations. After antigen coating and blocking, 25 μL of serially diluted non-biotinylated competitor antibody was added to each well at a concentration of 100, 10, 1, and 0.1 μg/mL, and incubated at 37°C for 10 min. Then, without washing, 75 μL of biotinylated antibody (final well concentration of 0.1 μg/mL) was added and incubated at 37°C for 1 h. After washing three times with PBS-T, streptavidin-HRP was added at a dilution of 1:10,000 in 1% milk in PBS-T and incubated for 1 h at room temperature. The plates were washed, and substrate and sulfuric acid were added as described earlier. ELISAs were repeated at least 2 times. Data is shown as the percentage decrease in binding relative to no competitor.

Real-time cell analysis (RTCA) neutralization assay

To determine neutralizing activity of IgG, Fab, or F(ab′)2 proteins, we used real-time cell analysis (RTCA) assay on an xCELLigence RTCA MP Analyzer (ACEA Biosciences Inc.) that measures virus-induced cytopathic effect (CPE).[45] Briefly, 50 μL of cell culture medium (DMEM supplemented with 2% FBS) was added to each well of a 96-well E-plate using a ViaFlo384 liquid handler (Integra Biosciences) to obtain background reading. A suspension of 18,000 Vero-E6 cells in 50 μL of cell culture medium was seeded in each well, and the plate was placed on the analyzer. Measurements were taken automatically every 15 min, and the sensograms were visualized using RTCA software version 2.1.0 (ACEA Biosciences Inc). VSV-SARS-CoV-2 (0.01 MOI, ∼120 PFU per well) was mixed 1:1 with a dilution of mAb in a total volume of 100 μL using DMEM supplemented with 2% FBS as a diluent and incubated for 1 h at 37°C in 5% CO2. At 16 h after seeding the cells, the virus-mAb mixtures were added in replicates to the cells in 96-well E-plates. Triplicate wells containing virus only (maximal CPE in the absence of mAb) and wells containing only Vero cells in medium (no-CPE wells) were included as controls. Plates were measured continuously (every 15 min) for 48 h to assess virus neutralization. Normalized cellular index (CI) values at the endpoint (48 h after incubation with the virus) were determined using the RTCA software version 2.1.0 (ACEA Biosciences Inc.). Results are expressed as percent neutralization in a presence of respective mAb relative to control wells with no CPE minus CI values from control wells with maximum CPE. RTCA IC50 values were determined by nonlinear regression analysis using Prism software.

SARS-CoV-2 VSV-G virus production

The generation of a replication-competent VSV expressing SARS-CoV-2 S protein with a 21 amino acid C-terminal deletion that replaces the VSV G protein (VSV-SARS-CoV-2) was described previously.[44] The S protein-expressing VSV virus was propagated in MA104 cell culture monolayers (African green monkey, ATCC CRL-2378.1) as described previously,[44] and viral stocks were titrated on Vero E6 cell monolayer cultures. VSV plaques were visualized using neutral red staining. All work with infectious SARS-CoV-2 was performed in Institutional Biosafety Committee approved BSL3 and A-BSL3 facilities at Washington University School of Medicine using appropriate positive pressure air respirators and protective equipment.

Pseudovirus production and neutralization assays

Lentiviral pseudovirus production and neutralizations were done in one of two different ways.

(1) For the pseudoviruses D614G, BA.2, BA.5, BA.4.6, BA.2.75.2, XBB, BQ.1.1, and XBB.1.5: HEK293T cells and HEK293T-hACE2 (stably expressing human ACE2) cells were cultured in Dulbecco's Modified Eagle Medium (high glucose, with sodium pyruvate) supplemented with 10% fetal bovine serum, 100 units/ml Penicillin, and 100 μg/mL Streptomycin. Cultures were maintained in a humidified 37C incubator (5% CO2). SARS-CoV-2 spike-pseudotyped lentiviruses were generated by the co-transfection of HEK293T cells with a spike-encoding plasmid (with a 19 amino acid C-terminal truncation), a lentiviral packaging plasmid (Addgene #8455), and a transfer plasmid encoding firefly luciferase (Addgene #170674) using polyethylenimine (PEI). Growth media was replaced 12–16 h after transfection, and pseudotyped viruses were harvested from the supernatant at 48- and 72-h post transfection, clarified by centrifugation, and stored at −80C. Pseudotyped viruses previously titrated to generate ~100,000 relative light units (RLUs) were incubated with serial 3-fold dilutions of antibody for 60 min at 37C, and then ~10,000 HEK293T-hACE2 cells were added to each well. Plates were incubated at 37C for 44–48 h and luminescence was then measured using Bright-Glo (Promega) on a GM-2000 luminometer (Promega) per the manufacturer's instructions. Neutralization was calculated relative to the mean of eight control wells infected in the absence of antibody and fit using a four-parameter logistic curve in Prism v9 (GraphPad Software).

(2) For the pseudovirus BA.2.75 + R346T: Lentiviral pseudoviruses bearing the S glycoproteins of SARS-CoV-2 variants were generated using a previously described protocol.[66] Briefly, HEK-293T/17 cells (ATCC, cat. CRL-11268) were seeded in a culture flask at a density that would give approximately 50–70% confluency on the day of transfection. The morning of the transfection, media was changed to fresh DMEM supplemented with sodium pyruvate, penicillin/streptomycin 25 mM HEPES, and 10% (v/v) FBS. To generate lentiviral-based reporter pseudoviruses, cells were co-transfected with a pHAGE-CMV-Luc2-IRES-ZsGreen-W plasmid encoding the lentiviral genome (BEI Resources, cat. NR-52516), the lentiviral packaging plasmids HDM-Hgpm2 (BEI Resources, cat. NR-52517), HDM-tat1b (BEI Resources, cat. NR-52518), and pRC-CMV- Rev (BEI Resources, cat. NR-52519), and a plasmid encoding the SARS-CoV-2 S gene with a 21 amino acid deletion. Approximately 16–18 h later, media was removed and replaced with fresh DMEM supplemented with sodium pyruvate, penicillin/streptomycin 25 mM HEPES, and 2% (v/v) FBS. Approximately 48 h after transfection, the supernatant was collected from each flask, clarified by centrifugation, and filtered through a 0.2 μm filter. Aliquots of pseudovirus stocks were prepared and stored at −80°C.

Lentivirus-based pseudoviral neutralization assays were executed based on a previous described protocol.[66] One day prior to the assay, HEK-293T cells transduced to stably express human ACE2 (293T-hACE2 cells, BEI Resources NR-52511) were seeded at a density of 1.25 × 104 cells per well in DMEM+10% FBS onto 96-well tissue culture plates that had previously been coated with poly-D-lysine (ThermoFisher Scientific, cat. A3890401) The day of the assay, monoclonal antibodies were diluted in DMEM+2% FBS using a 4-fold dilution series (with each antibody in technical duplicate) in a 96-well polypropylene microtiter plate and incubated with pseudovirus for 1 h at 37°C in the presence of a final concentration of 5 μg/mL polybrene (EMD Millipore). After the 1 h incubation, pseudovirus-mAb mixtures were added to 293T-hACE2 monolayers. Plates were incubated at 37°C for 48–60 h, at which point cells were lysed using the Bright-Glo Luciferase Assay System (Promega) and luciferase activity was quantified using a CLARIOStar plate reader (BMG LabTech). The luminescence signal from wells in each plate where no pseudovirus or antibody was added was averaged and subtracted from each value, after which the percent infection of each well was determined relative to the average of pseudovirus only control wells present in each plate. IC50 values were determined by nonlinear regression using Prism v.9.5 (GraphPad) using a four-parameter [inhibitor] vs. response curve fit with top and bottom values constrained to 100 and 0, respectively. Each neutralization assay was repeated twice.

Public antibody analysis

For generation of plots for each child antibody in comparison with previously published adult antibodies with respective to percent CDRH3 (x axis) and percent CDRL3 (y axis) identity, CovAbDab database was used.[50] Each dot is colored according to V-gene usage: blue if both the VH and VL of the given child and adult antibodies match, orange if only the VH match, purple if only the VL match, and gray if neither match but at least either one of the CDRH3 or CDRL3 have ≥50% sequence identity for the child vs. adult antibody.

Sequences and gene annotations for antibodies in clinical use were manually curated from IMGT/3Dstructure-DB[67] and compared to the SARS-CoV-2 antibodies from children using a custom Python script. Heavy chain CDR3 identity between each antibody pair was defined by calculating the Levenshtein distance between the amino acid sequences and dividing by the length of the longer CDR3 region.

Negative stain electron microscopy (nsEM) sample and grid preparation, imaging and processing of spike–Fab complexes

To perform electron microscopy imaging, Fabs were produced by digesting recombinant chromatography-purified IgGs using resin-immobilized cysteine protease enzyme (FabALACTICA, Genovis). The digestion occurred in 100 mM sodium phosphate and 150 mM NaCl pH 7.2 (PBS) for around 16 h at ambient temperature. To remove cleaved Fc from intact IgG, the digestion mix was incubated with CaptureSelect Fc resin (Genovis) for 30 min at ambient temperature in PBS buffer. Spike protein were incubated with the Fab at an Fab:S protein molar ratio of 4:1 for about 1 h at ambient temperature, and approximately 3 μL of the sample at concentrations of

about 10–15 μg/mL was applied to a glow-discharged grid with continuous carbon film on 400 square mesh copper electron microscopy grids (Electron Microscopy Sciences). The grids were stained with 2% uranyl formate.[68] Images were recorded on a Gatan US4000 4k×4k CCD camera using an TF20 transmission electron microscope (TFS) operated at 200 keV and control with Serial EM.[69] All images were taken at 50,000× magnification with a pixel size of 2.18 Å/pixel in low-dose mode at a defocus of 1.5–1.8 μm. The total dose for the micrographs was around 30e− per Å2. Image processing was performed using the cryoSPARC software package.[62] Images were imported, CTF-estimated and particles were picked. The particles were extracted with a box size of 256 pixels and binned to 128 pixels (4.36 Å/pixel). 2D class averages were performed and good classes selected for *ab initio* model and NU refinement without symmetry with final resolution of ~20 Å. Model docking to the EM map was done in ChimeraX.[63] For spike protein model (PDB:7XIW) was used and PDB:12E8 was used for the Fab. ChimeraX software was used to make all figures, and the EM map has been deposited into EMDB (EMD-41075, EMD-41076).

QUANTIFICATION AND STATISTICAL ANALYSIS

The ELISA error bars (± standard error of the mean) were calculated using Graphpad Prism 9.5.0. Mean ± SEM or mean ± SD were determined for continuous variables as noted. Technical and biological replicates are described in the figure legends. Details of the statistical analysis can be found in the main text and respective figure captions.